

THE TRENDS HIGH-CONTRAST IMAGING SURVEY. IV.
THE OCCURRENCE RATE OF GIANT PLANETS AROUND M-DWARFS

BENJAMIN T. MONTET¹, JUSTIN R. CREPP², JOHN ASHER JOHNSON^{3,4}, ANDREW W. HOWARD⁵, GEOFFREY W. MARCY⁶
Draft version December 8, 2018

ABSTRACT

Doppler-based planet surveys have discovered numerous giant planets with short orbital periods but are currently incomplete beyond several AU. At larger star-planet separations direct planet detection through high-contrast imaging has proven successful, but this technique is sensitive to only the youngest planets and characterization relies upon theoretical evolution models which are poorly constrained. Here we demonstrate that a combination of precise radial velocity measurements and high-contrast imaging can be used to overcome these issues. The presence of widely separated companions can be deduced by identifying an acceleration (long-term trend) in the radial velocity of a star as only a small fraction of its orbit is observed. By obtaining high spatial resolution follow-up imaging observations, we rule out scenarios in which such accelerations are caused by stellar binary companions with high statistical confidence. We report results from an analysis of Doppler measurements of a uniform sample of 111 M-dwarf stars with a median of 29 radial velocity observations over a median time baseline of 11.8 years. By targeting stars that exhibit a radial velocity acceleration (“trend”) with adaptive optics imaging, we determine that $6.5\% \pm 3.0\%$ of all M dwarf stars have a gas giant companion with $1M_J < m < 13M_J$ and $a < 20$ AU, and that there are 0.083 ± 0.019 planets in this parameter space per M-dwarf star. These results are lower than previous analyses of the planet occurrence rate around higher mass stars. Additionally we find a strong correlation between giant planet occurrence and stellar metallicity inside of the M-dwarf spectral class. Our results are consistent with gravitational microlensing measurements of the planet occurrence rate; this study represents the first model-independent comparison with microlensing observations.

Subject headings: methods: observational—planets and satellites:detection, fundamental parameters—techniques: radial velocities, high angular resolution

1. INTRODUCTION

Over the past twenty years, numerous planets have been detected by several different techniques, permitting the first estimates of the occurrence rate of planets orbiting stars in the solar neighborhood (e.g. Johnson et al. 2010b; Howard et al. 2010b; Gould et al. 2010; Vigan et al. 2012). As successful as these detection methods have been, each is sensitive only to a relatively narrow range of parameter space. For example, radial velocity (RV) studies are most sensitive to massive planets with small orbital periods. Wright et al. (2012) calculate that $1.20\% \pm 0.38\%$ of FGK stars host a “hot Jupiter” with mass larger than $m \sin i > 0.1M_J$ and period shorter than 10 days. By analyzing stars with longer period RV signals, Johnson et al. (2010b) find that $3.4_{-0.9}^{+2.2}\%$ of M dwarfs have a Saturn-mass or larger planet within 2.5 AU; this frequency increases with increasing stellar mass

and metallicity. Beyond a few AU, RV searches are incomplete as the time required for a planet to complete one orbit is longer than the typical observing baseline. Some studies have attempted to extrapolate beyond this boundary. For instance, Cumming et al. (2008) fit the observed RV planet population to a power law in planet mass and period and find that $18\% \pm 1\%$ of FGK stars host a Saturn-mass or larger planet within 20 AU.

Transit studies suffer from similar detection biases. Since a planet transits only once each orbit, several orbits must be observed to definitively confirm a planet so characterization is limited to planets with periods shorter than a fraction of the observing baseline (Gaudi et al. 2005). Additionally, the probability of a planet transiting its host star decreases with increasing orbital period (Winn 2011), such that hundreds of thousands of stars must be monitored in order to study the planet population at $a \approx 1$ AU (Borucki & Summers 1984). Nevertheless, the success of the *Kepler* mission (Borucki et al. 2010; Koch et al. 2010) has allowed for statistical analyses of transiting planets to be undertaken. For example, Morton & Swift (2013) analyze M dwarfs included in the 2012 list of announced Kepler Objects of Interest (KOIs, Batalha et al. 2013). By correcting for false positives (detections when no transiting planet exists), false negatives (nondetections when a transiting planet is present) and geometric effects (nondetections of non-transiting planets), they estimate an occurrence rate of 1.5 planets per M dwarf star, slightly higher than previous studies which find occurrence rates of one planet per

btm@astro.caltech.edu

¹ Cahill Center for Astronomy and Astrophysics, California Institute of Technology, 1200 E. California Blvd., MC 249-17, Pasadena, CA 91125, USA

² Department of Physics, University of Notre Dame, 225 Nieuwland Science Hall, Notre Dame, IN 46656, USA

³ Division of Geological and Planetary Sciences, California Institute of Technology, 1200 E. California Blvd., MC 170-25, Pasadena, CA 91125, USA

⁴ NASA Exoplanet Science Institute (NExSci), CIT Mail Code 100-22, 770 South Wilson Avenue, Pasadena, CA 91125, USA

⁵ Institute for Astronomy, University of Hawaii, 2680 Woodlawn Drive, Honolulu, HI 96822, USA

⁶ B-20 Hearst Field Annex, Astronomy Department, University of California, Berkeley, Berkeley, CA 94720, USA

star (Youdin 2011; Mann et al. 2012; Swift et al. 2013; Dressing & Charbonneau 2013).

Neither RV nor transit searches are yet conducive to the discovery and characterization of planets well beyond the “snow line,” where water exists as ice. Instead, high contrast direct imaging techniques can be a powerful tool for detecting young planetary companions in this domain. The first direct imaging planet discoveries are securely in hand, including four companions to HR 8799 (Marois et al. 2008, 2010) and one each around β Pictoris (Lagrange et al. 2009), and G1 504 (Kuzuhara et al. 2013)⁷. Recent studies using these techniques have calculated an occurrence rate around A stars of $8.7_{-2.8}^{+10.1}\%$ at 1σ confidence for planets larger than $3M_J$ and separations between 5 and 320 AU (Vigan et al. 2012). Imaging studies have been most effective around high mass stars. (Crepp & Johnson 2011; Carson et al. 2013). Nondetections around lower-mass stars have been used to place upper limits on the frequency of giant planets. For example, Nielsen & Close (2010) rule out the presence of giant planets orbiting FGKM stars beyond 65 AU with 95% confidence. High contrast imaging, while powerful, only provides a measure of the relative brightness of a companion. To estimate the companion’s mass, the age of the star must be known and planetary thermal evolution models must be applied to estimate the temperature (and brightness) of the companion (Chabrier et al. 2000; Baraffe et al. 2003). Moreover, direct imaging is currently only sensitive to massive planets; the HR8799 planets and β Pic b are believed to have masses $m > 5M_J$. RV and transit studies suggest such “super-Jupiters” are rare compared to Jovian-mass and smaller objects at smaller separations (Howard et al. 2010b, 2012).

The gravitational microlensing technique is also effective for finding giant planets in wide orbits and does not rely on planetary evolution models. Using this technique, planets can be detected by observing perturbations to the photometric gravitational microlensing signal when a planet and its host pass in front of a more distant star. Since 70 – 75% of stars in the galaxy are M-dwarfs, most lenses have mass $M < 0.5M_\odot$. Microlensing searches thus provide a measure of planet occurrence around low mass stars. Microlensing studies are sensitive to planets near the Einstein ring, $R_E \sim 3.5\text{AU}(M/M_\odot)^{1/2}$, a much wider separation than RV and transit searches. Gould et al. (2010) find microlensing searches are most sensitive to planets at a projected separation in the range $[s^{-1}R_E, sR_E]$, where $s \sim (q/10^{-4.3})^{1/3}$ and q is the mass ratio between a companion and the host star. These authors find a planet occurrence rate that can be parameterized by a double power-law function, in mass ratio q and separation s , such that

$$\frac{d^2N}{d \log q d \log s} = (0.36 \pm 0.15) \left(\frac{q}{5 \times 10^{-4}} \right)^{-0.60 \pm 0.20} \text{dex}^{-2}. \quad (1)$$

With additional data, Cassan et al. (2012) update this result to find a normalization constant of

⁷ Companions detected around Fomalhaut (Kalas et al. 2008), HD 95086 (Rameau et al. 2013), and LaCa15 (Kraus & Ireland 2012) are also good candidates to be directly imaged planets, but their true nature is somewhat ambiguous.

$10^{-0.62 \pm 0.22} (0.24_{-0.10}^{+0.16})$ and a power-law slope in mass $d^2N/(d \log q d \log s) \propto q^{-0.73 \pm 0.17}$. Both results assume planets are distributed uniformly in $\log s$, as is the case for binary stars (Öpik 1924). Additionally, Sumi et al. (2010) find a power-law slope in mass such that $dN/d \log q \propto q^{-0.68 \pm 0.20}$ for Neptune-sized planets, but do not attempt to quantify a normalization factor.

The physical parameters of planets found in targeted searches are usually not measured directly, but instead measured in relation to their host stars. As microlensing studies focus on distant M-dwarfs ($d > 1$ kpc) in the direction of the galactic bulge (Gaudi et al. 2002), these stars can be difficult to characterize accurately due to crowding. Stellar masses and metallicities are often estimated without being measured. If these host stars have different masses than assumed, it would affect the results of planet occurrence rate studies by microlensing groups as microlensing results do not account for correlations between stellar and planet properties. Additionally, as microlensing searches are most sensitive near $r = R_E$, beyond approximately 10 AU the lensing signal becomes very weak, and differentiating distant planets from unbound, “free-floating” planets becomes difficult (Sumi et al. 2011).

RV and microlensing studies probe different regions around a star, and extrapolations between the two domains suggest a possible discrepancy. Cumming et al. (2008) studied the statistics of the Keck/HIRES Doppler survey and found that $18 \pm 1\%$ of FGK dwarfs have a planet at least as massive as Saturn within 20 AU, lower than the predictions offered by microlensing results. Derived power-law distributions in mass may also be different for planets found by each method: Cumming et al. (2008) find a distribution such that $dN/d \log m \propto m^{-0.31 \pm 0.20}$ from RV-detected planets, different from the Cassan et al. (2012) result by 1.6σ . Since giant planet occurrence decreases with decreasing stellar mass and metallicity (Johnson et al. 2010a), the expected giant planet occurrence rate around M dwarfs would be smaller than that for FGK stars. Therefore, it is necessary to compare the microlensing planet population not to a population of FGK stars, but instead to a study of RV detected planets around M-dwarfs.

Historically, RV observations have been used to detect and characterize planets once they complete a full orbit, limiting studies to planets with periods shorter than the observing time baseline. In this paradigm, potentially useful information is overlooked. Wide companions are not completely undetectable: instead they can be identified by the presence of long-term RV accelerations (linear “trends”) and can provide information about planets in more distant orbits (Liu et al. 2002; Crepp et al. 2012a). In other words, the existence of an acceleration can be used to infer the existence of a companion in a wide orbit. However, a linear acceleration does not provide unique information about the mass and period of the companion: the same trend could be caused by a Jupiter-mass planet at 5 AU or a $100M_J$ M-dwarf at 25 AU. This degeneracy can be broken by adaptive optics (AO) imaging. Low-mass binary stars in wide orbits around nearby M-dwarfs can be easily imaged by modern AO systems (Lloyd 2002; Siegler et al. 2003; Crepp et al. 2012b).

In this work, we combine RV and AO observations of

nearby cool stars to estimate the frequency of giant planets in wide orbits around M-dwarfs. From a sample of 111 M-dwarfs observed with a median Doppler RV baseline of 11.8 years, we identify 4 systems with long-term RV accelerations but no known companions and target these stars with AO imaging in an attempt to detect binary star companions. Given an observed RV trend or lack thereof, we determine with high statistical confidence if a giant planet exists around each star. We analyze the effects of false positive and false negative detections of RV accelerations in our sample, then estimate the occurrence rate of giant planets around M-dwarfs and compare the result to results from other techniques. This study represents the first measurement of the planet population in the range 0–20 AU. While we rely on brown dwarf cooling models, our study does not make use of theoretical planetary evolution models, unlike other AO studies of planetary systems.

The paper is organized as follows. In §2 we discuss the methodology for target selection and explain the RV and AO imaging observations collected. In §3 we discuss possible detection biases and astrophysical effects that could cause a false positive or false negative detection in our sample, and their effect on the results. In §4 we present our results and compare to other studies. We summarize and conclude in §5.

2. SAMPLE AND OBSERVATIONS

2.1. Target Selection

Since 1997, the California Planet Search (CPS) collaboration has undertaken a comprehensive Doppler search for extrasolar planets at the Keck Observatory (e.g. Howard et al. 2010a). Using Keck/HIRES (Vogt et al. 1994), the CPS program monitors over 2000 stars, most selected to be chromospherically quiet, single, and bright. Included in this sample is a collection of M-dwarfs from the Gliese and Hipparcos catalogs brighter than $V = 11.5$ and lacking known stellar companions within 2 arcseconds (Rauscher & Marcy 2006). This sample was later extended to $V = 13.5$ and currently includes 131 M-dwarfs within 16 pc of the Sun, where we define the M spectral class as targets with $B - V > 1.44$.

To develop the sample used here, we first remove from this set 20 stars with a known, nearby binary companion. We define “nearby” as a separation small enough that a test particle orbit with semimajor axis ≥ 30 AU would be unstable, following the instability criterion of Holman & Wiegert (1999). This criterion depends on the unknown eccentricity of the binary pair, as perturbative effects are maximized at periapsis. We take $e = 0.5$ as a typical value and find the onset of instability occurs for binary stars with $a \sim 250$ AU. Planets can still form in these more compact binary systems (e.g. Gl667C; Anglada-Escudé et al. 2012b) but at such small separations protoplanetary disk formation and planet evolution would be affected significantly by the presence of stellar companions. This selection thus allows us to study a class of planets that likely followed similar evolutionary processes. Moreover, the detection of an acceleration around these stars is ambiguous, as it could be caused by the binary star, a planetary-mass companion, or both together.

After making the above selection we are left with 111

RV targets, all of which have at least 8 radial velocity observations and a time baseline longer than 2.9 years. The median number of observations is 29 over a median time baseline of 11.8 years. The stars have spectral types from M0 to M5.5 and masses in the range $0.64M_{\odot} - 0.10M_{\odot}$. Stellar masses are estimated using the empirical relation between mass and absolute K-band magnitude, M_K , described by Delfosse et al. (2000). We take 10% as a typical uncertainty in the stellar mass, in line with previous estimates (Bean et al. 2006). K-band apparent magnitudes are measured using apparent magnitudes from the 2MASS point-source catalog (Cutri et al. 2003). The majority of our parallaxes are taken from an analysis of *Hipparcos* data (van Leeuwen 2007). Some of our stars were not observed by *Hipparcos*, while others have had their distances updated more recently. In these cases, we apply the distances listed in the SIMBAD astronomical database (Table 1). For example, for Gl317 we use the parallax found by Anglada-Escudé et al. (2012a); their derived mass and metallicity are consistent with our estimated values. In all cases, stellar metallicities are estimated by measuring the offset between the star’s position in the $\{V - K_s, M_{K_s}\}$ plane from a calibrated main sequence following the method of Neves et al. (2012). We take 0.17 dex as a typical uncertainty in the stellar metallicity, representative of the scatter between this photometric method and spectroscopic measures of stellar metallicity. Stellar and observational parameters for these targets are listed in Table 1 and the distribution of RV observational parameters are shown in Fig. 1. RV observations for a representative sample of six “typical” stars are shown in Fig. 2.

2.2. Detecting Accelerations from Radial Velocities

The detection of a long-term RV acceleration is facilitated by having many observations over a long time baseline to increase signal, but complicated by astrophysical “jitter” caused by rotational modulation of surface inhomogeneities. To determine the masses and semimajor axes to which we are sensitive to planetary companions, we inject a series of artificial companions into orbit around the stars in our sample. We define a grid of companion masses and semimajor axes spanning the range $0.75M_J < m < 100M_J$ and $3\text{AU} < a < 30\text{AU}$. At each point, we inject 500 planets and randomly assign each of the remaining orbital elements. The longitude of ascending node Ω , time of periapsis t_p , and argument of periapsis ω are drawn from a uniform distribution, while the inclination is drawn from a distribution $dn/di = \sin i$ and the eccentricity from a distribution such that $dn/de = 1 - e$, which well-replicates the distribution of observed eccentricities for RV planets with orbits longer than 10 days (Johnson 2009). We then numerically integrate these orbits forward in time over our true observing baseline.

At the epochs each star was observed by CPS, we measure the expected radial velocity signal caused by our injected planet. Each velocity is perturbed from the true expected Keplerian velocity by a normal variate with zero mean and standard deviation σ representative of the total expected noise:

$$\sigma = \sqrt{\sigma_{\gamma}^2 + \sigma_{\text{jitter}}^2}. \quad (2)$$

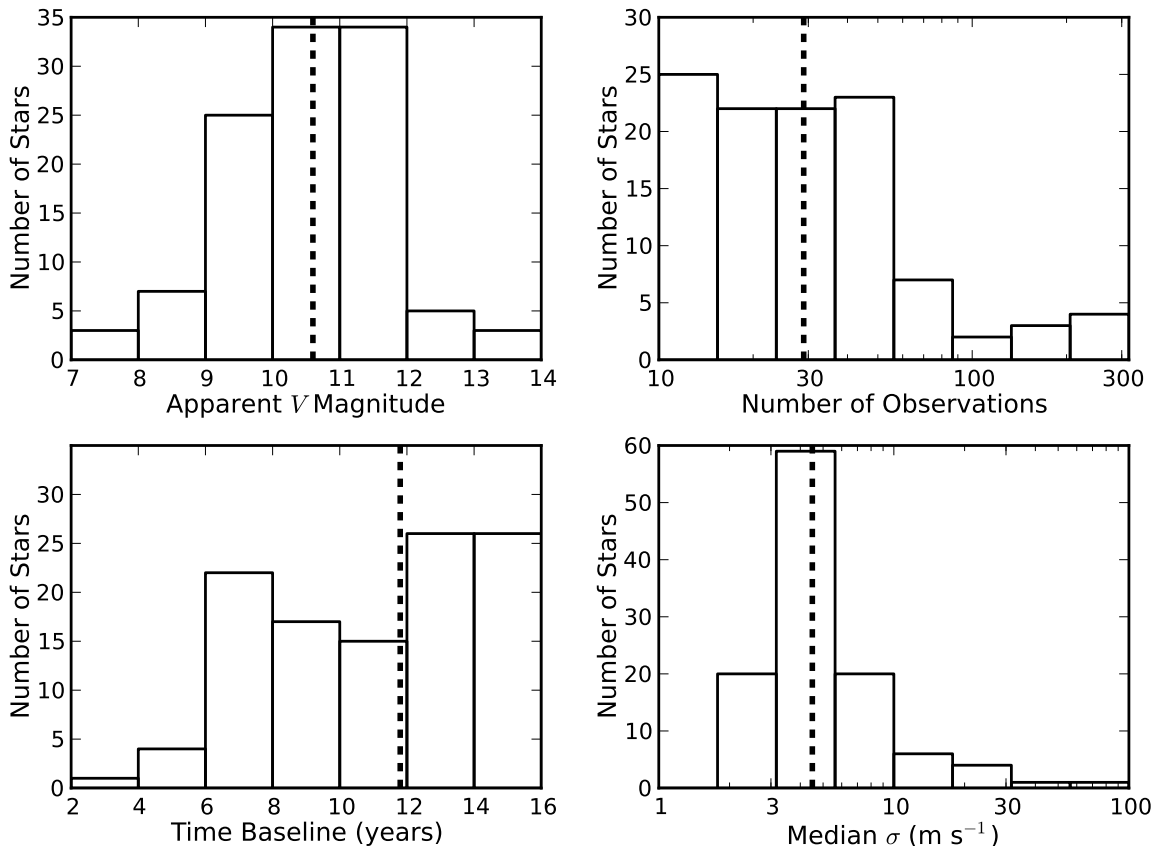


FIG. 1.— Distributions of the RV observational parameters. Dashed lines represent the median values for each parameter. The median target brightness is $V = 10.6$, and the median target has been observed 29 times over 11.8 years. The median measurement uncertainty σ , defined as the sum in quadrature of rotational jitter and statistical uncertainty (Eq. 2) is 4.5 m s^{-1} . Specific parameters for each individual system are shown in Table 1.

Here, σ_γ is the photon noise, estimated by randomly selecting a measurement of the true Poisson photon noise from an actual observation of the star. To account for the effects of jitter, we follow the method of Isaacson & Fischer (2010), who develop an empirical relation between the level of stellar jitter, a star’s S_{HK} value, and its $B - V$ color. S_{HK} is defined as the ratio of the flux in the Ca II line cores to flux in the surrounding continuum. We compare the S_{HK} value observed by CPS to that expected from the star’s $B - V$ color, which provides an estimate of σ_{jitter} . This value is added in quadrature to the photon noise to estimate a total observational uncertainty, σ .

Once all observations are accounted for, we search for evidence of our injected planetary companion, manifested as an acceleration in the RV data. Here, we define the existence of a trend using the Bayesian Information Criterion (BIC; Schwarz 1978; Bowler et al. 2010; Campo et al. 2011; Stevenson et al. 2012), which prefers simple, well-fitting models subject to

$$\text{BIC} \equiv -2 \ln \mathcal{L} + k \ln N, \quad (3)$$

where \mathcal{L} is the maximum likelihood for a model with k free parameters and N observations. The BIC thus favors models that fit the underlying data well, but penalizes

increasingly complex models. For a more complex model to be preferred by the BIC, it must improve the fit by an amount greater than $k \ln N$ to overcome the penalty term.

Jeffreys (1961) claim a BIC value greater than 10 (corresponding to a Bayes factor of 0.01) suggests strong evidence for an association between two parameters. If the BIC value decreases by more than 10 when considering a model with a linear acceleration over a model with only an offset, a planet is considered to be detected. Otherwise, the system is considered a non-detection. We find that the ΔBIC value chosen here is consistent with by-eye inspection of our data in a visual search for RV accelerations. By repeating this process for many simulated planets over our mass-semimajor axis grid, we can map out the relative probability of detecting a linear trend caused by a planet as a function of companion mass and semimajor axis. As an example, Fig. 3 shows RVs for HIP 70975 and the likelihood of detecting a planet at a given mass and period given these observations. Fig. 4 shows the mean likelihood of detecting a planet around a given star across our sample. We are able to detect many, but not all, planets larger than $m = 1M_J$ with a semimajor axis below 20 AU. Throughout this work, we report the occurrence rate of planets with masses in the

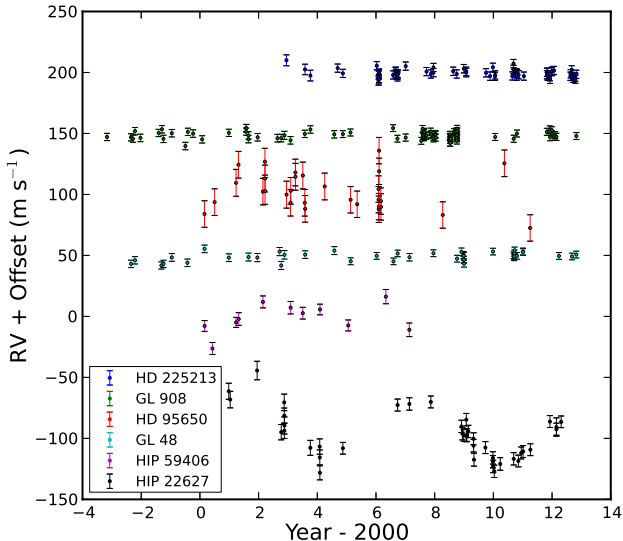


FIG. 2.— RV measurements for a representative sample of six example stars. The stars are arranged such that the brightest star is at the top of the plot. The individual stars vary considerably with respect to observing baselines, measurement uncertainty, and number of observations. Of these stars, HIP 59406 has a wide binary companion, while HIP 22627 has both a known inner planet and long-term RV acceleration.

range $1M_J < m < 13M_J$. We can detect accelerations caused by planets smaller than $1M_J$ in certain instances, but would miss the majority of these planets. As Fig. 4 shows, we can only detect a $0.75M_J$ planet at 6 AU 50% of the time; planets at smaller separations would exhibit significant curvature over a 12 year time baseline and could be detected through an RV survey alone. We are more efficient at detecting planets larger than $1M_J$, although we would still not expect to detect all planets in this range. We account for false negative “missed” planets in our analysis, as described in §3.1.

Seven of the stars in our sample host known planets inside of 2 AU, all of which have $m \sin i < 2.5M_J$. To identify radial velocity accelerations caused by outer planets, we include the signal from these planets by comparing a model which contains the known planet and an acceleration to a model which contains only the known planet. Two known planets in our sample, Gl 876b and Gl 317b, are larger than $1M_J$, so despite subtracting out the signal in a search for long-term accelerations, we include these planets in our analysis.

One additional planet, HIP 109388b, has a best-fitting mass $m \sin i = 0.90 \pm 0.05M_J$; if the inclination is smaller than 64 degrees this planet has mass $m > 1M_J$. We follow the method of Ho & Turner (2011) to determine the probability of this event. Determining the likelihood of a given inclination requires an assumption of the underlying mass distribution function, which is randomly selected following the distribution found by Cumming et al. (2008), as explained in §3.3. By assuming the star is aligned randomly along our line of sight so that the inclination distribution is flat in $\cos i$, we expect a observed mass $m \sin i = 0.90M_J$ to be produced by a Jupiter-mass or larger planet 56% of the time; all reasonable assumptions of an underlying mass distri-

bution affect this value by less than 10%. We repeat this procedure for all confirmed planets in our sample to quantify the likelihood that other known planets are $m > 1M_J$ planets with low inclinations. We find, in addition to HIP 109388b, HIP 22627b ($m \sin i = 0.64M_J$) has approximately a 25% probability of having a mass $m > 1M_J$. This probability is vanishingly small for all other known planets.

Of our sample of 111 stars, 2 have confirmed planets larger than $1M_J$, 4 systems have confirmed RV planets with $m \sin i < 1M_J$, two exhibit RV acceleration caused by known brown dwarfs, and four show unexplained long-term RV accelerations. In the case of HIP 109388b, the long-term acceleration exhibits significant curvature, so we are able to place constraints on this object’s mass and orbital semimajor axis. In all other cases, the magnitude of the observed acceleration is different from zero by 3σ . Additionally, the magnitude of the acceleration is such that over the observing baseline, the expected ΔRV induced by the putative outer planet is larger than the uncertainties of each individual data point. The distribution of these systems in the stellar mass-metallicity plane is shown in Fig. 5.

For the four targets with an observable RV drift, we create a grid of logarithmically-spaced companion masses and semimajor axes over the range $0.75 < m/M_J < 100$ and $3AU < a < 30AU$. For a given grid point, we determine the best-fitting Keplerian orbit for a given eccentricity and inclination. We assume the inclination and eccentricity distributions are the same as assumed in §2.2. The eccentricity distribution is well-characterized for solar-type stars, but may not hold for planets around lower-mass stars. We find the exact choice of eccentricity distribution does not significantly affect our results.

We determine the likelihood of the best-fitting orbit for each mass, period, eccentricity, and inclination. We then convert these likelihoods into relative probabilities, assuming our errors are uncorrelated. We then marginalize over eccentricity and inclination and normalize our probabilities so that $\sum_{M,a} P = 1$. The result is a contour

in the mass-semimajor axis plane for the likelihood that a given object could cause the observed stellar radial velocity variation (Wright et al. 2007). An example is shown in Fig. 6. Implicit in this analysis is the assumption the radial velocity variation is dominated by the motion of a single, massive companion rather than the constructive interference of the RV signal of two or more smaller objects. We discuss false positive probabilities in §3.2 and conclude the assumption that one signal dominates the observed RVs is reasonable.

The magnitude of an acceleration depends on both the semimajor axis and mass of the companion. For a planet in a circular orbit, the magnitude of the change in radial velocity, $\dot{\gamma} = dv/dt$, is given by

$$\dot{\gamma} = (6.57 \text{ m s}^{-1} \text{ yr}^{-1}) \left(\frac{m_p}{M_J} \right) \left(\frac{a}{5\text{AU}} \right)^{-2} \hat{v}_p \cdot \hat{r}_{los}, \quad (4)$$

with M_J the mass of Jupiter and a the orbital semimajor axis. \hat{v}_p and \hat{r}_{los} are unit vectors along the direction of the planet’s velocity vector and the line of sight, respectively. When the companion has longitude of periapsis $\varpi = 90$ or 270 , the magnitude of this trend is maxi-

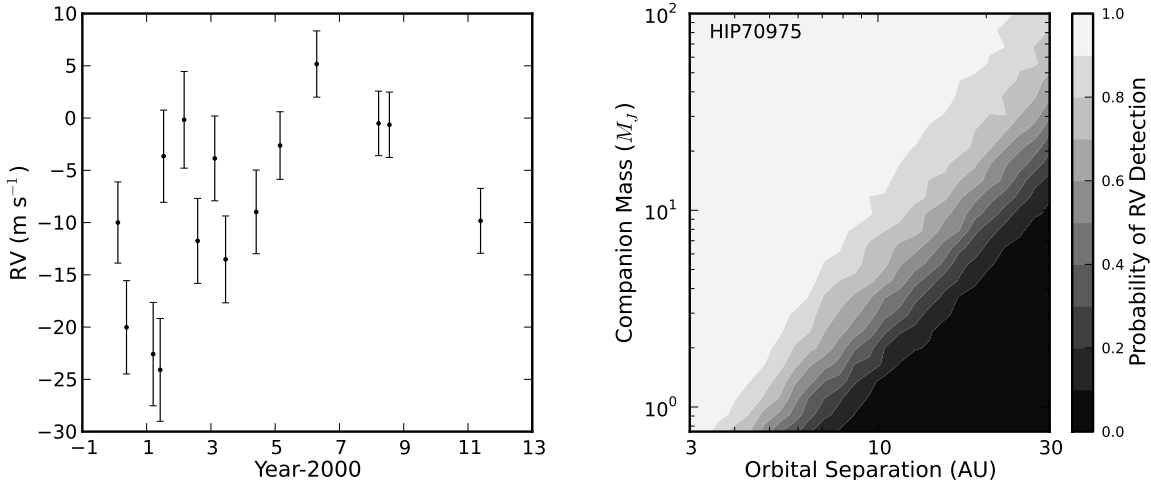


FIG. 3.— (left) RVs for HIP 70975, a typical star in our survey. This $0.32M_{\odot}$ M-dwarf has a total of 15 radial velocity observations over a baseline of 15.5 years, with an average RV precision (including photon noise and jitter) of 4 m/s. (right) Detectability plot showing the likelihood of an RV detection for a companion orbiting HIP 70975 as a function of companion mass and semimajor axis from its host star.

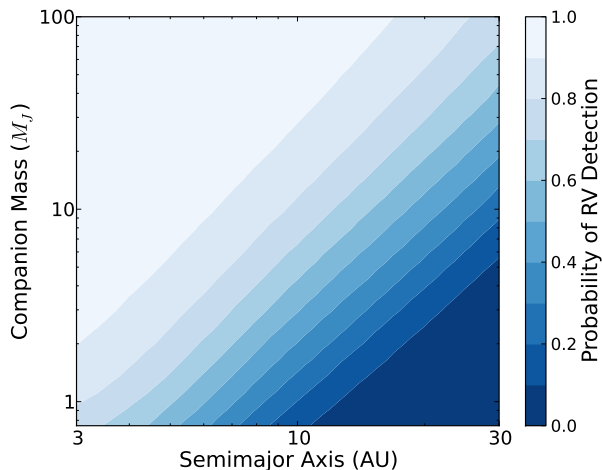


FIG. 4.— The ensemble average likelihood over all 111 stars of an RV detection for a companion to a star in our sample as a function of companion mass and orbital semimajor axis. We can detect accelerations induced by planets as small as $1M_J$ in short orbits, but a planet distribution function is required to determine the number of $1M_J$ planets in wide orbits and calculate the overall giant planet occurrence rate.

mized: $\hat{v}_p \cdot r_{los} = \sin i$. In this case, a degeneracy between the companion’s mass $m \sin i$ and orbital semimajor axis exists: a $1M_J$ gas giant planet at 5 AU could produce the same acceleration as a $100M_J$ companion at 25 AU. To determine if our observed accelerations are caused by planets or more massive companions, we obtained AO imaging observations of each star.

2.3. Adaptive Optics Observations

The detectability diagnostics developed in §2.2 are based strictly on the information encoded in the RV data. Since we are looking at accelerations caused by objects in wide orbits around the primary star, we must break the degeneracy between companion mass and orbital semimajor axis for a given observed acceleration. AO imaging allows us to immediately detect the presence or nonexistence of nearly all stellar-mass companions and most

brown dwarf companions to our primary stars, so we can readily separate stellar-induced accelerations from those caused by planets.

Each target was observed with NIRC2 (instrument PI: Keith Matthews) at the W.M. Keck Observatory using the AO system (Wizinowich et al. 2000) (Table 2). In most cases, images were obtained in the K' filter ($\lambda_c = 2.12\mu\text{m}$). We nominally execute a three-point dither pattern to facilitate removal of instrument and sky background noise. Images were processed by flat-fielding, correcting for hot pixels with interpolation, subtracting the sky background, and rotating the frames to standard north-east orientation. In three cases, we applied the angular differential imaging (ADI) point spread function subtraction technique, allowing the observed field to rotate around the target star during the observation, while instrumental artifacts remain fixed. In all cases, we use the large hexagonal pupil mask and the narrow camera. For all four systems exhibiting long-term RV accelerations, we did not image a massive companion. In the cases where our field of view is not large enough to eliminate the possibility of massive stars in very wide orbits ($> 4''$), we supplement our AO data with publicly available 2MASS images.

The luminosity ratio between our M-dwarfs and their companions depends on the mass of the companion and the age of the system. Stars observed by the CPS team are selected to avoid excessive chromospheric activity, and are thus likely older than 1 Gyr (Wright 2005). We assume all targets have fully contracted and assert an age of 5 Gyr for each system. For systems with nondetections, we estimate the flux (and thus the mass) a companion would need to have to be observed at a given projected separation in our observations. From that value, we can then determine the region of parameter space excluded by the observations (Fig. 6). In general, AO imaging eliminates nearly all stellar companions, while ADI can also probe the brown dwarf mass regime.

For each of our targets with unexplained accelerations, a contrast curve showing the mass to which we are sensitive to companions at the 5σ level as a function of pro-

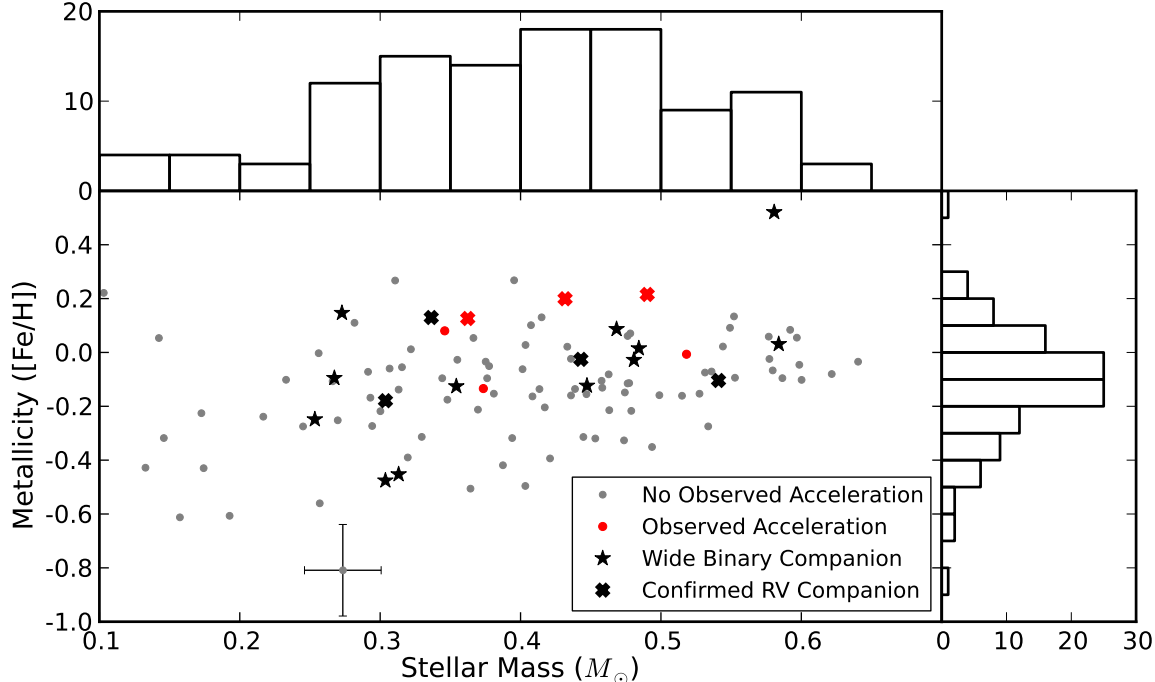


FIG. 5.— Observed M-dwarf sample in the stellar mass-metallicity plane. Systems with observed RV accelerations are shown in red while those without a detected acceleration are in black. Systems with a wide binary companion are labeled with stars, while diamonds represent systems with confirmed planets of any mass. The error bars displayed for HD 33793 are representative of the uncertainties for all stars in our sample.

jected separation is shown in Fig. 7. This choice provides similar results to the detection limits found by visual inspection, as tested by injecting artificial companions into AO images (Metchev & Hillenbrand 2009). We convert relative brightness to mass using the theoretical evolutionary tracks of Baraffe et al. (2003) for substellar companions and ? for more massive companions. Interpolation between the two sets of models provides reasonable results in the intermediate domain near $125M_J$. The resultant parameter space where a companion could reside to cause the observed stellar acceleration is shown in Fig. 6.

The assumption of a 5 Gyr age for each star does not significantly affect our results. For all plausible system ages, stellar mass companions would be easily detectable by AO. Our sensitivity to stars is independent of assumed age, as luminosities of M-dwarfs are constant over the age of the universe. At no ages > 1 Gyr are we sensitive to any planetary mass companions. As shown in Fig. 8, assuming a different age for each star would only change the efficiency of detecting brown dwarfs. Since the occurrence rate of brown dwarfs is only a few percent, much smaller than the occurrence rate of planets or low-mass stars (Metchev & Hillenbrand 2009; Dieterich et al. 2012), errors induced by assuming an incorrect stellar age from missed brown dwarfs are small. “False negatives” such as these will be discussed in §3.1.

3. MEASURING THE GIANT PLANET OCCURRENCE RATE

We estimate the occurrence rate of giant planets orbiting M-dwarfs using statistical inference. The fraction of stars which host giant planets, given some number of observed accelerations N_{trends} and some number of non-

detections N_{ND} from a sample of targets, is given such that

$$f_{pl} = \frac{N_{\text{trends}}P(\text{planet}|\text{trend}) + N_{\text{ND}}P(\text{planet}|\text{ND})}{N_{\text{targets}}} \quad (5)$$

To calculate the posterior probability that a given star hosts a gas giant planet, we must estimate the *a priori* likelihood that such a planet would not be detected in an RV survey (a false negative) and the likelihood that an observed acceleration is caused by some effect other than the movement of a planet (a false positive).

3.1. False Negatives

There are multiple ways for a giant planet to be missed in our survey. For each planet in a wide orbit, we observe only a fraction of a revolution. A planet near its maximal sky-projected separation from its host star has acceleration primarily in the tangential, not radial, direction. In cases such as this the change in radial velocity over our observing baseline may not be noticeable. Thus we may expect to have a lower RV detection efficiency for planets near their maximal sky-projected separation.

To determine the likelihood that such a planet would be missed by our search, we use our detectability matrices developed in §2.1. We assume the distribution of planets follows a double power-law, such that

$$\frac{d^2N}{d \log m d \log a} \propto m^\alpha a^\beta, \quad (6)$$

similar to that assumed by Cumming et al. (2008) and Bowler et al. (2010), and comparable to the power-law distributions applied in the analyses of microlensing surveys. At a given companion mass and semimajor axis, we

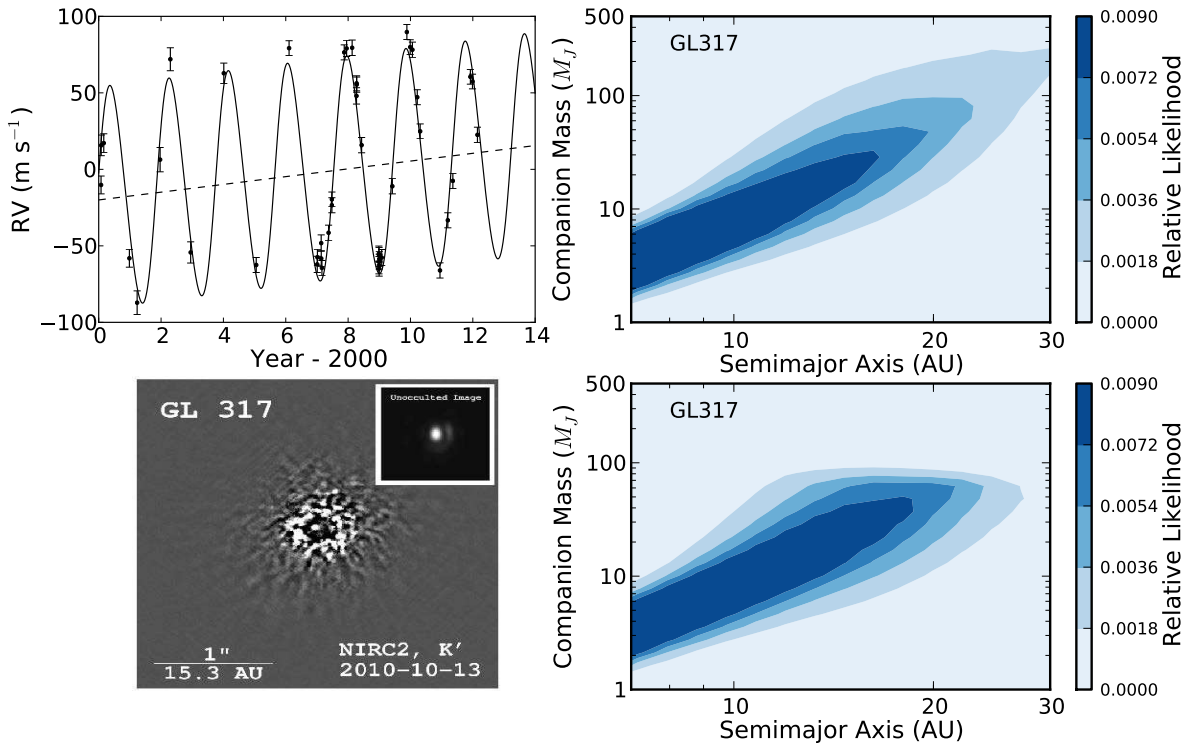


FIG. 6.— (top left) RV observations for Gl317 over our 12.1 year baseline. The orbit for Gl317b is shown as a solid line, while the best-fitting RV acceleration is $-2.51 \pm 0.62 \text{ m s}^{-1} \text{ yr}^{-1}$ (dashed line). (top right) Probability contours marginalized over eccentricity and inclination, displaying the location of a giant companion orbiting Gl317 from RVs alone. The likelihood values are normalized such that the sum of the likelihood over our 26×25 grid of companion masses and separations sums to unity. (bottom left) AO image of Gl317, showing no companion is visible in the AO imagery, either in the unocculted image (inset) or when a coronagraph is inserted. This eliminates the possibility of a stellar-mass companion at a projected separation smaller than 48 AU. (bottom right) Probability contours displaying the location of a giant companion to Gl317 when the RV data is combined with AO data. We find the RV acceleration is likely induced by a substellar companion.

can then determine the relative likelihood that a planet exists at this position. We multiply this by the likelihood of detecting such a planet to determine the fraction of planets we would find orbiting each star and the fraction we would miss. These numbers are determined through our analysis of observations of simulated injected planets, as developed in §2.1.

We can test our detectability calculation by analyzing the known wide-separation companions in our sample. Of our 111 stars, four are known to host directly imaged brown dwarf companions. Of these, two (HD 71898B and HIP 63510B) were detected as accelerations in our sample, while two (Gl 569B and HD 42581B) are at very large separations and were not detected. The detection or non-detection of each system is consistent with what would be expected from our analysis of injected planets (see Appendix).

We detect the two brown dwarfs with high expected RV detection efficiency, and do not detect the two with expected detection efficiencies near zero, both of which have $a > 40 \text{ AU}$. We would like a larger sample to test this method, but the limited number of brown dwarfs suggests our ability to detect giant planets is consistent with expectations. This sample also suggests f_{BD} is only a few percent, consistent with complementary studies (Dieterich et al. 2012).

A giant planet could also be missed if it was in a system with multiple giant planets. We observe only the sum of all radial velocity signals from all planets orbiting a star. For example, if a star hosts two giant long-period planets with one on each side of the star, the two signals would destructively interfere. Even if the acceleration was still detectable, this interference would cause us to measure an incorrect magnitude of the acceleration, so our probability contours would be incorrect. Giant planet multiplicity around M-dwarfs is not well understood, but since giant planet occurrence is believed to be small (Bonfils et al. 2013) the multiplicity rate of giant planets around M-dwarfs is likely also small. Presently, there are no known systems with two planets larger than Jupiter orbiting one M-dwarf. Even in cases with two large planets, one planet will dominate the RV signal. For example, OGLE-2006-BLG-109L contains a $0.73 M_J$ planet near 2.5 AU and a planet less massive than Saturn near 4.5 AU (Gaudi et al. 2008). In this case the Doppler amplitude of the inner planet would be a factor of 3.3 larger than the Doppler amplitude of the outer planet. Similarly, an external observer of the solar system would observe an RV signal from Jupiter 4.5 times larger than that of Saturn. Thus we neglect this possible source of error.

We then claim that the likelihood of the existence of a

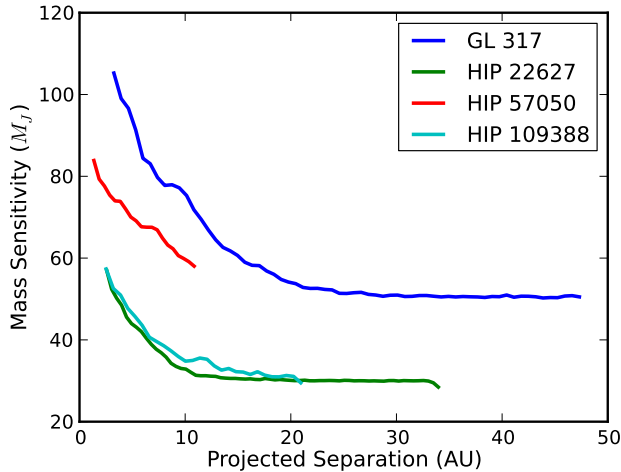


FIG. 7.— Mass sensitivity for a 5σ detection of a companion object as a function of projected angular separation for each of our four stars with long-term RV drifts. The maximum projected separation eliminated corresponds to the field of view of the AO system and thus varies for each star as a function of the distance to each star. For all stars except HIP 57050, we rule out stellar mass companions beyond 1 arcsecond through our adaptive optics imaging. When our field of view is small, we supplement our AO data with 2MASS seeing-limited images. Stellar companions at small projected separations would have RV accelerations larger than those observed in our sample.

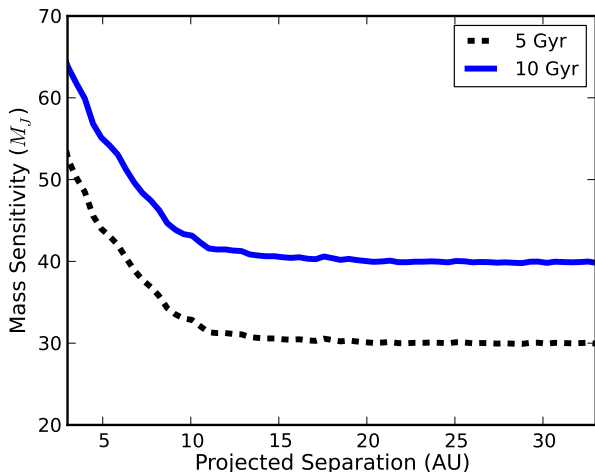


FIG. 8.— Adaptive optics mass exclusion plot for the star HIP 22627 showing the relative insensitivity of our results to the assumed age of M-star planet hosts. Adaptive optics observations rule out essentially all stellar mass companions. Sensitivity to sub-stellar objects is a function of age, but brown dwarfs are scarce at close separations (Marcy & Butler 2000), and wide separations (Metchev & Hillenbrand 2009). Thus, our estimate of the planet frequency around M-stars is only weakly dependent on our assumed age of the host stars.

giant planet given the nondetection of an RV acceleration is

$$P(\text{planet}|\text{ND}) = f_{pl}(1 - \eta_{pl,*}) \quad (7)$$

where $\eta_{pl,*}$ is our detectability efficiency of detecting a giant planet around a given star. The probability of missing a planet depends on the true giant planet occurrence rate, f_{pl} . We can determine this value directly if the underlying planet distribution function (Equation 6) is as-

sumed. By counting the observed trends and analyzing our RV detection efficiencies for each star as a function of mass and separation, we can determine the number of missed planets. We find our final result is not a strong function of mass index α or semimajor axis index β (see §4.6).

3.2. False Positives

3.2.1. Multiple Planets

In some cases, observed accelerations may not be induced by the orbit of a giant planet. If two smaller planets are orbiting one star, when they are both on the same side of the star their RV signals would constructively interfere, giving the appearance of a giant planet where none exists. Again, multiplicity rates of large planets are unknown for these small stars but are likely small; we again neglect this effect as a possible source of error. This is a reasonable assumption even if the multiplicity rate of gas giant planets around M-dwarfs was much larger than currently expected. Both the orientation of the system and the relative positioning of the planets during our observations is random. Therefore, it is equally likely that multiple planets would be in the “constructive” or “destructive” phase of their orbits. Thus, similar numbers of false additional planets would be added to our sample as missed true planets.

3.2.2. Secular Acceleration

A false positive can also be caused by secular acceleration. When a high proper motion star moves quickly relative to the Sun, its peculiar velocity vector changes direction in time, causing the star’s systemic radial velocity to increase. For a star with proper motion μ at a distance d the magnitude of this effect is, to first order,

$$\dot{\gamma} = 23.0 \text{ cm s}^{-1} \text{ yr}^{-1} \left(\frac{d}{10 \text{ pc}} \right) \left(\frac{\mu}{1 \text{ arcsec yr}^{-1}} \right)^2. \quad (8)$$

The secular acceleration $\dot{\gamma}$ is always positive, so that the star’s radial velocity only increases because of this effect. For several nearby stars secular acceleration is large enough to create an apparent acceleration or cause an astrophysical RV acceleration to be incorrectly measured. For example, Barnard’s star has a secular acceleration of $4.515 \pm 0.002 \text{ m s}^{-1} \text{ yr}^{-1}$ (Choi et al. 2013), larger than all of our observed accelerations. Fortunately, the magnitude of the secular acceleration can be precisely quantified if the star’s distance and proper motion are known. All of our stars have measured proper motions and parallaxes, so we can determine the expected secular contribution. This acceleration is subtracted from the observed radial velocity automatically by the CPS RV pipeline (Howard et al. 2010a), so this potential source of error is automatically accounted for in our data. Moreover, none of our observed accelerations are consistent with what would be expected from secular acceleration alone.

3.2.3. Magnetic Activity

Magnetic activity on a star can cause a false positive: rotating active regions can affect the shape of the observed spectral lines and thus the apparent RV (Gray 1988). A magnetic cycle can occur over years and hide

or mimic a radial velocity signal. We denote the fraction of stars with a magnetically-induced acceleration as f_A . Gomes da Silva et al. (2012) claim six stars from their sample of 14 M-dwarfs with variability ($43\% \pm 17\%$) have RVs induced by magnetic activity. We are interested in the converse (how many trends are induced by variability?) but their result suggests f_A may be significant. To determine f_A , we review all M-dwarfs observed by the CPS team, both as part of this survey and as part of the M2K survey (Apps et al. 2010; Fischer et al. 2012). Between these two programs, there are a total of 34 systems with RV trends. We analyze the S_{HK} values for these stars and find the RV correlates with S_{HK} with a correlation coefficient $|r| > 0.5$ in 7 cases, suggesting $20.6\% \pm 7.8\%$ of long-term RV trends may be magnetically induced. We adopt this value as f_A . Even if the true value for f_A is a factor of two larger, it would decrease our planet occurrence rate from $f_{pl} = 6.5\%$ to only $f_{pl} = 4.9\%$, still within our uncertainties.

3.2.4. Brown Dwarfs

Our adaptive optics search is sensitive to all stellar-mass companions, but only to the most massive brown dwarfs. We can detect brown dwarfs larger than approximately $50M_J$, although this number varies from target to target. For each target, we can determine the fraction of brown dwarfs we would expect to detect by our adaptive optics imaging, given the assumption that a trend was caused by a brown dwarf. We call this efficiency η_{BD} . Here, we assume a form for the brown dwarf mass function where $dn/d\log(m) \propto m^{0.4 \pm 0.2}$ (Peña Ramírez et al. 2012). Thus we can estimate the likelihood of detecting a brown dwarf around a star in our sample, given that a brown dwarf exists. To estimate the probability a brown dwarf exists, we use the result of Dieterich et al. (2012), who, through an HST/NICMOS snapshot program, estimate that $f_{BD} = 2.3^{+5.0}_{-0.7}\%$ (at 1σ) of M-dwarfs have an L or T companion between 10 and 70 AU. This is consistent with the result of Metchev & Hillenbrand (2009), who estimate a brown dwarf companion frequency of $f_{BD} = 3.2^{+3.1}_{-2.7}\%$ (at 2σ) around solar-type (FGK) stars.

3.2.5. White Dwarfs

Compact stellar remnants are often faint and such binary companions can evade direct detection, especially when the compact object is cool ($T < 4000K$) so that the infrared light is dominated by the primary star (Crepp et al. 2013). Since our targets are all M-dwarfs, it is not unreasonable to expect that some may have formed as lower mass companions in binary systems with the higher mass object having evolved off the main sequence to become a white dwarf. Napiwotzki (2009) combine observations of local white dwarfs with galactic structure models and find that in the thin disk there is a white dwarf number density of $n_{WD} = 2.9 \times 10^{-3} \text{ pc}^{-3}$. From an analysis of PanSTARRS data, Wheeler (2012) estimate 20% of all white dwarfs have an M-dwarf companion ($f_{M|WD}$), somewhat larger than the 12% found by Napiwotzki (2009). Considering the measurement by Chang et al. (2011) of $n_{\star} = 0.030 \pm 0.002$ stars per cubic parsec, and that approximately 70% of all stars are M-dwarfs ($f_{M|\star}$, Henry et al. 2006), we can determine the fraction of M-dwarfs in the thin disk with a white dwarf

companion, a number we define as f_{WD} . We find that

$$f_{WD} = \frac{n_{WD} f_{M|WD}}{n_{\star} f_{M|\star}} = 2.5\% \pm 0.5\%. \quad (9)$$

By combining the false positive events from §3.2.3, §3.2.4, and §3.2.5, we conclude that given the existence of a trend in our data, the likelihood it is caused by a giant planet is

$$P(\text{planet}|\text{trend}) = (1 - f_A)[1 - f_{BD}(1 - \eta_{BD,\star})](1 - f_{WD}) \quad (10)$$

3.3. Determining f_{pl}

We determine the giant planet occurrence rate, f_{pl} by combining our estimate of the number of false positives and false negatives with the number of observed accelerations. Specifically, the occurrence of giant planets is given by Eq. 5 if the number of observed accelerations is known, along with the probability of a false negative or false positive in our sample. These probabilities are defined by Equations 7 and 10, respectively.

For each star in our sample, we use our map of giant companion detectability (e.g. Fig. 6) to estimate our efficiencies, η_{BD} and η_{pl} . We measure the total planet fraction, f_{pl} and its uncertainty through a Monte Carlo experiment. For each trial, we establish an expected number of observed accelerations, drawing from a binomial distribution with $n = 111$ and $p = 4/111$, representing the most likely underlying distribution behind our observed sample. In practice, we draw from our star list 111 times, with replacement, to determine a stellar sample. We then draw randomly from our previously defined distributions to estimate f_A , f_{BD} and f_{WD} . These values are sufficient to calculate the probability an observed acceleration is caused by a false positive astrophysical event. In cases where known planets with masses $m > 1M_J$ exist in our sample, we include their presence in our calculation of f_{pl} .

The derivative of the RV acceleration (the ‘‘jerk’’) for HIP 109388 is nonzero, so we can use the RV information to fit a two-planet model to this system, instead of a planet plus a linear acceleration (see Appendix). We find the inner planet to have a mass $m \sin i = 0.90 \pm 0.05M_J$ with a period of 5.24 ± 0.07 years, and the outer planet to have a mass $m \sin i = 0.70 \pm 0.31M_J$ with a period of $19.3^{+17.1}_{-5.9}$ years. More data is needed to determine the exact parameters of the orbit of HIP 109388c, but from the existing RV information we can determine the probability each planet has a mass $m > 1M_J$. The exact value depends on the planet mass distribution function; assuming each orientation has equal probability (so that $\alpha = -1$) we find probabilities of 0.577 and 0.419, respectively. Following the method of Ho & Turner (2011), we find changing the distribution function changes these values by less than 10%.

Since we know the region of mass-separation parameter space to which we are sensitive to planets for each star, we can self consistently estimate the planet frequency in this parameter space. We then assume the result from Cumming et al. (2008), who find the power-law indices (Eq. 6) of $\alpha = -0.31 \pm 0.20$ and $\beta = 0.39 \pm 0.15$. We randomly select values for α and β from these distributions and use our detection efficiencies to determine the

number of false negative missed planets in our sample. Through Equation 5, we then have enough information to estimate the planet fraction as a function of each parameter. By repeating this process many times, varying each of our assumed parameters, we can measure the overall planet fraction and its uncertainty.

4. RESULTS AND DISCUSSION

4.1. The Frequency of Giant Planets

Given an observed trend, we can estimate the likelihood the signal is caused by a massive planet. By analyzing our 111 targets as described in §3.3, we recover a distribution in giant planet occurrence as shown in Fig. 9. We find from this analysis that $6.5\% \pm 3.0\%$ of all M-dwarfs host a giant planet with a semimajor axis smaller than 20 AU. This number is lower than previous studies of higher-mass stars. Bowler et al. (2010) find $24_{-7}^{+8}\%$ of “retired” A stars host Jupiter-mass planets within 3 AU, while Cumming et al. (2008) find that $f_{pl} = 10\% \pm 1\%$ of FGK stars host Jupiter-mass planets within 20 AU.

If we consider multiplicity in situations where we have a giant planet and an RV acceleration (or in the case of HIP 109388, two giant planets), then we measure a giant planet occurrence rate of 0.083 ± 0.019 giant planets per star.

Our result is consistent with the result of microlensing surveys of M-dwarfs, which suggest a total occurrence rate of $0.09_{-0.05}^{+0.03}$ giant planets per star in the range $1M_J < m < 10M_J$ and $0.5 \text{ AU} < a < 20 \text{ AU}$ Cassan et al. (2012). However, the power-law distribution determined by the microlensing studies is considerably different than the Cumming et al. (2008) distribution assumed here. We discuss this further and constrain α and β in §4.7.

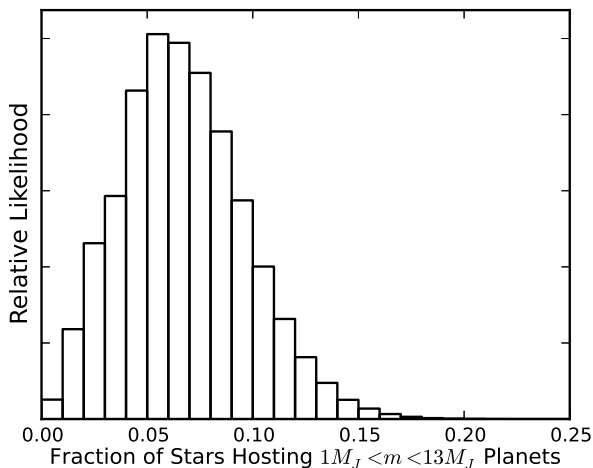


FIG. 9.— Giant planet occurrence for our sample of 111 nearby M-dwarfs. We find $6.5\% \pm 3.0\%$ of M-dwarfs host a planet with mass $1M_J < m < 13M_J$ and $a < 20 \text{ AU}$.

4.2. Potential Missed Binary Stars

We only collect AO images for systems with long term RV accelerations. For these accelerations to be observable, the orbiting companion must have a component of its orbit along our line of sight. A giant planet would

be missed if it was in a near face-on orbit, such that the star’s reflex motion was primarily in the plane of the sky. Such systems are accounted for in our detectability calculations (Fig. 3), as we have determined the probability of detecting a planet’s RV acceleration as a function of its mass and separation, marginalizing over all other orbital parameters. These calculations do not, however, account for the possible presence of close stellar binary companions in face-on orbits. Although less common than edge-on systems, any missed binary systems that we have not rejected from our sample would cause our planet occurrence rate to be artificially low (assuming these systems could not form dynamically stable planets). Close binaries would be observable as double-lined spectroscopic systems (SB2s) in the CPS data, while wider binary pairs would be easily imaged by AO systems.

The RV sample was originally selected to reject systems with known binary companions within 2 arcseconds. We would expect companions with a flux ratio larger than 0.01 ($\Delta V = 5$) to be detected as binaries (Robinson et al. 2007). For our brightest targets, this would correspond to M6 dwarfs and brighter. As the cutoff for hydrogen burning is the M6 spectral class (Luhman 2012), we would expect all close stellar-mass binaries to be removed from our HIRES observations.

To determine how many missed binaries are in our sample, we simulate a population of binary companions to M-dwarfs. We create binary companions such that their semimajor axes are assigned following the observed distribution found by Fischer & Marcy (1992). We randomly assign the other orbital parameters and determine there is a $41.8\% \pm 0.3\%$ chance a binary companion in our sample around a random star would have a projected separation smaller than two arcseconds. Thus, considering Fischer & Marcy (1992) find $42\% \pm 9\%$ of local M-dwarfs are in binary or multiple systems, we would expect to have a total of 26 ± 6 binary systems in our sample. As we actually observe 22 binary systems (containing 26 stars), this result is consistent with our expectation.

We then determine the radial velocity each simulated binary star would induce on our host companion. For each binary that induces a measurable acceleration on the host star, we simulate imaging observations to determine the probability this binary companion would be detected in either our AO survey or, for very wide separation binaries, a seeing-limited ground based survey such as 2MASS. By applying our joint AO/seeing-limited contrast curves, we find that if a binary star system in our survey induces an RV acceleration, we would have a $96.0\% \pm 0.4\%$ chance of imaging this binary companion. Therefore the probability that one or more of our observed accelerations is caused by a “missed” binary companion is negligible and this possibility does not significantly affect our results.

4.3. Dependence on Stellar Mass

Previous RV studies have found a correlation between stellar mass and giant planet occurrence at $a < 2.5 \text{ AU}$, with more massive stars more likely to host giant planets (Johnson et al. 2010a). To test this relation inside the M-dwarf spectral class, we analyzed the high mass stars separately from the low mass stars in our sample. From our best fit masses, half of our sample is more massive than $M = 0.41M_\odot$. We thus use this value as a dividing

line to separate our sample into two groups. Our masses have typical uncertainties of 10%, so for each star, given its mass and uncertainty, we determine the probability it is larger or smaller than $0.41M_{\odot}$ assuming normally distributed errors. We then use that value as a weighting factor to assign a probability for each individual star to reside in our high mass or low mass bin, and then repeat our analysis for each individual subsample.

We find an occurrence rate for the high mass subsample of $4.8 \pm 3.3\%$ and for the low mass subsample of $7.9 \pm 4.2\%$ (Fig. 10). Johnson et al. (2010a) find planet occurrence is correlated with stellar mass such that $f_{pl} \propto 10^{(1.2 \pm 0.2)[Fe/H]} M_{\star}^{(1.0 \pm 0.3)}$. The average star in our high-mass sample has a mass of $0.5 M_{\odot}$ while the average star in our low-mass sample has a mass of $0.3 M_{\odot}$, so we would expect the high-mass subsample to have an occurrence rate larger than the low-mass sample by a factor of 1.67. We find the true occurrence rate to change by a factor of 0.61 ± 0.87 in moving from the lower-mass to higher-mass bin. This is inconsistent with the expected result from Johnson et al. (2010a), but the difference between the two bins is not significantly different from zero. A larger sample is required to determine if the small difference between these two populations of M-dwarfs is real or the result of a statistical anomaly. However, our result is lower than the Cumming et al. (2008) result for FGK stars, that $f_{pl} = 10\% \pm 1\%$ of FGK stars host Jupiter-mass planets within 20 AU. This difference is consistent with the Johnson et al. (2010a) correlation between stellar mass and planet occurrence.

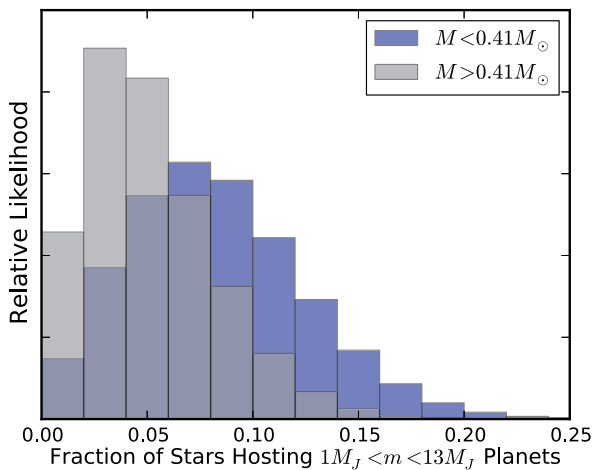


FIG. 10.— Planet occurrence for a low mass subsample (blue) and a high mass subsample (gray) of M dwarfs. Both subsets have nearly similar giant planet occurrence rates, suggesting planet occurrence may not depend strongly on stellar mass within the M spectral class. A larger sample is required to determine if the lack of difference in occurrence rates is astrophysical or statistical variance.

4.4. Dependence on Metallicity

Previous RV studies of giant planets have also found evidence for a correlation between planet occurrence and metallicity. To test if this correlation holds for more distant planets, we again split our sample into two, using the same method from the previous section. In this case,

we use $[Fe/H] = -0.10$, the sample median metallicity, as the dividing line for our subsamples. We assume all stars have metallicity uncertainties of 0.17 dex, consistent with the scatter expected from the Neves et al. (2012) empirical relation. Again, we assume Gaussian errors to determine the probability each star is in a specific subsample. We then repeat our analysis on both groups.

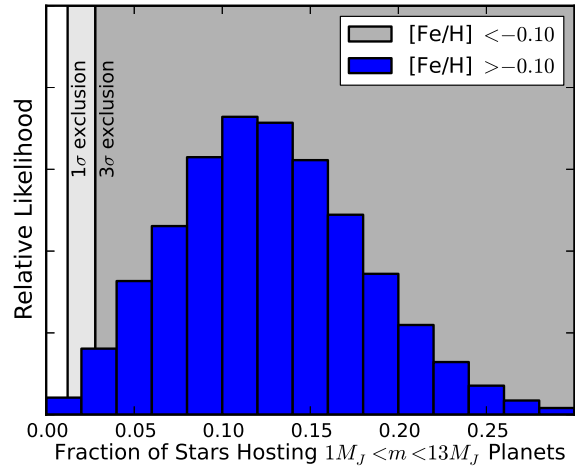


FIG. 11.— Planet occurrence for a high metallicity subsample (blue) and 1 and 3σ exclusion regions for a low metallicity subsample (gray) of M dwarfs. The high metallicity sample has a significantly higher occurrence rate than the low metallicity sample, similar to the phenomenon observed for RV-detected planets.

In the high-metallicity subsample, we find an occurrence rate such that $12.4 \pm 5.4\%$ of M-dwarfs host giant planets. In the low metallicity sample the occurrence rate drops to $0.96 \pm 0.51\%$. In Fig. 11 we plot a histogram of our posterior distribution of planet occurrence for our high-metallicity subsample. Vertical lines represent (from left to right) 1 and 3σ upper limits on the planet fraction. From these distributions, the giant planet occurrence rate for metal-rich stars has only a 2.4% probability of being lower than the 3σ upper limit on the planet occurrence rate for metal-poor stars. The difference between these subsamples may be suggestive of the same effect seen for RV-confirmed planets within 2.5 AU (Johnson & Apps 2009; Johnson et al. 2012). An increase in the planet occurrence rate with metallicity for planets beyond a few AU may suggest giant planets in wide orbits are commonly formed by the same processes as the RV giant planet population. This study will be facilitated by the development of reliable spectroscopic metallicity measurements (Rojas-Ayala et al. 2010).

4.5. The Effect of Distant Binary Companions

In the above analysis, we neglect binary stars where a test particle at 30 AU would be in an unstable orbit, but include 10 binaries at wider separations. Although these systems formally allow stable orbits, Kaib et al. (2013) suggest these orbits can change significantly over time. Because the binary pair is weakly bound, interactions with the galactic tidal field or nearby passing stars can vary the binary orbit. The binary can then strongly perturb formerly stable planetary companions, potentially resulting in the ejection of planets from the system within

5 Gyr, our estimated age for the M-dwarfs in our sample. None of our 10 wide binary systems show evidence for an RV acceleration, providing weak but tantalizing evidence in favor of this theory. If we repeat our analysis but neglect these stars as potential hosting systems, we find that $7.2\% \pm 3.2\%$ of single stars host giant planets, compared to $6.5\% \pm 3.0\%$ of our full sample. With zero detections in a sample of 10 wide binaries, we can only place an upper limit of $f_{pl} \leq 0.26$ at 95% confidence on the occurrence rate of giant planets in wide binary systems. With more observations of stars with wide binary companions, the occurrence rate of planets orbiting true field stars can be compared to the rate for wide binaries.

4.6. Sensitivity to Power-Law Parameters

The result for f_{pl} is dependent on the assumed planetary distribution function, as that function determines the number of missed (false negative) planets in our sample. To quantify the dependence of the planetary occurrence rate on our choice of α and β we repeat our analysis over a grid of values for α and β . The giant planet occurrence rate as a function of these two parameters is shown in Fig. 12. We find that there is only a weak relation between α and f_{pl} in the range $-2.0 < \alpha < 0.5$, where we might reasonably expect α to reside. f_{pl} depends more strongly on β , but our overall result does not change by more than 1σ by selecting any β in the range $-1.0 < \beta < 1.0$ for a given α . Selecting any α or β over this range affects our final result by less than a factor of two.

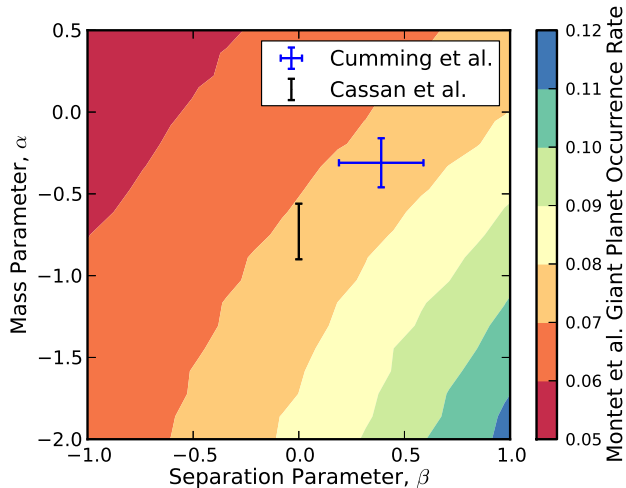


FIG. 12.— Giant planet occurrence rate, f_{pl} , as a function of the mass parameter index α and separation parameter index β . There is not a strong dependence on α or β ; selecting $\alpha < -1.0$ and $\beta > 0.5$ is required to affect our result at more than the 1σ level. Labeled points include the Cumming et al. (2008) result for FGK stars, with $\alpha = -0.31 \pm 0.15$ and $\beta = 0.39 \pm 0.15$, and the microlensing result of Cassan et al. (2012), who find $\alpha = -0.73 \pm 0.17$ and assume $\beta \equiv 0$.

From our sample of targets alone, we are unable to place constraints on acceptable values of α and β . To constrain α and β , the occurrence rate of giant planets at a given mass or separation is required. We have determined the bulk occurrence rate of planets, but cannot uniquely determine their properties. With continued

observations, as our RV accelerations “turn over” and become closed orbits, we will be able to determine the exact locations of giant planets around M-dwarfs and constrain the power-law parameters. Alternatively, we can constrain α and β by combining our results with those from microlensing observations.

4.7. Comparison with Microlensing Results

In §4.6, we showed that our bulk occurrence rate is not a strong function of α and β . However, the types and locations of our planets is a function of these parameters: if α is large, then most of our observed trends must be caused by large planets in wide orbits. Since microlensing results are most sensitive at projected separations corresponding to the Einstein radius, where $R_E \sim 3.5\text{AU}(M_*/M_\odot)^{1/2}$, we can compare our results to microlensing planet occurrence studies. As our results will only be consistent with microlensing estimates of the planet occurrence rate at the Einstein radius for specific values of α and β , comparisons between the two methods will enable us to constrain α and β .

To compare the two sets of results, we assume the population of M-dwarfs observed by microlensing studies is similar to that targeted by RV surveys in the local neighborhood. We find evidence for a correlation between giant planet frequency and metallicity in our sample, similar to that found by previous RV analyses of planets with $a < 2.5$ AU (Fischer & Valenti 2005; Johnson & Apps 2009). M-dwarfs studied by microlensing are at distances larger than 1 kpc and in the direction of the galactic bulge, along the galactic metallicity gradient (Rolleston et al. 2000). Measurements of the metallicity of Cepheids suggest the iron content in the disk varies such that $d[\text{Fe}/\text{H}]/dr = -0.051 \pm 0.004$ dex kpc^{-1} between 5 and 17 kpc from the galactic center (Pedicelli et al. 2009). Thus, the microlensing M-dwarfs may be more metal-rich than stars in the local neighborhood, so f_{pl} may be larger for the microlensing population than the RV population. Without spectra of galactic stellar planet-hosting lenses their true stellar properties are unknown. Programs dedicated to collecting spectra of galactic stellar planet-hosting lenses would greatly inform our knowledge of these stars and their planets.

If we assume the planet mass distribution function of Cumming et al. (2008), then from our analysis we would expect microlensing studies to measure a planet occurrence rate $f_{pl} = 0.056 \pm 0.023$ bound Jupiter-mass planets per star by analyzing signals from planets near the Einstein radius. Cassan et al. (2012) claim an occurrence rate of $10^{-0.62 \pm 0.22}$ ($0.24^{+0.16}_{-0.10}$) Saturn-mass planets at this separation. If we scale this occurrence rate to Jupiter-mass planets following the mass index observed in microlensing studies, $\alpha = -0.73 \pm 0.17$, then the observed microlensing density of Jupiter mass planets would be 0.101 ± 0.016 planets per star, different from our expectation at 1.6σ . If (and only if) the two populations have intrinsically similar occurrence rates of giant planets, then the difference between the number of planets found must be due to a planet distribution different from the one used by Cumming et al. (2008). As the RV planet distribution was developed from an analysis of FGK stars, it may not be surprising if the RV planet population is intrinsically different from the microlensing

planet population.

4.7.1. Joint Constraints on α

We depart from our previously assumed values of α and β to determine what values of α and β satisfy both our observed RV accelerations and the results of Cassan et al. (2012). We assume the planet occurrence rate presented by Cassan et al. (2012) is representative of the planet population at the Einstein radius. Moreover, we assume planet orbital semimajor axes are distributed uniformly in logarithmic space following Öpik’s Law ($\beta = 0$), as microlensing studies assume. This is slightly shallower than what is observed in the RV planet population ($\beta = 0.39 \pm 0.15$), but since the RV population of giant planets likely underwent considerable migration this may be a reasonable assumption. We then vary α , and for each value determine the space density of planets at 2.5 AU. We then compare our expected result to the result from Cassan et al. (2012), which we scale to Jupiter-mass planets according to our α parameter. We finally require $\alpha < 0$: despite the uncertainties in this mass parameter, previous studies agree that around M dwarfs, small planets are more common than massive planets (Swift et al. 2013; Morton & Swift 2013).

We find microlensing results agree with our result for f_{pl} when $\alpha = -0.94 \pm 0.56$ (Fig. 13). This result is consistent with the best-fitting values for α found by Gould et al. (2010) and Cassan et al. (2012). If we include the Cassan et al. (2012) result as a prior in our analysis, we find $\alpha = -0.77 \pm 0.22$. However, while our result agree with microlensing studies, our result for α is different from the Cumming et al. (2008) result for FGK stars at 1.1σ and significantly different from the Bowler et al. (2010) constraints for A stars, which rule out all $\alpha < 0.25$ with 90% confidence and all $\alpha < 1.75$ with 50% confidence. Since microlensing overpredicts the number of planets found at the Einstein radius relative to that expected by RV extrapolations, it is not surprising that we find a smaller value for α is required for our result to be consistent with the microlensing results: if the two populations are the same, there must be many low-mass giant planets below the simultaneous RV and imaging detectability limits than high-mass planets above the limits.

4.7.2. Simultaneous Constraints on α and β

We are not restricted to Öpik’s Law. We can allow both α and β to vary, and compare the normalization of Cassan et al. (2012) for Saturn-mass objects at 2.5 AU to our projected planet density at that mass and separation (Fig. 14). Performing this exercise, we find the most acceptable values of α and β are correlated approximately along the line $\alpha - \beta = -1$. That is, for every 1 dex increase in α , β must decrease by 1 dex to maintain a reasonable fit to both our result and the microlensing results.

4.7.3. A Model-Independent f_{pl}

We can apply these relative likelihood values as priors to the occurrence rate as a function of α and β shown as Fig. 12 to determine an occurrence rate independent of our choices of α and β , but dependent on the RV and microlensing stars both being representative of similar populations. We assume our separation parameter must be

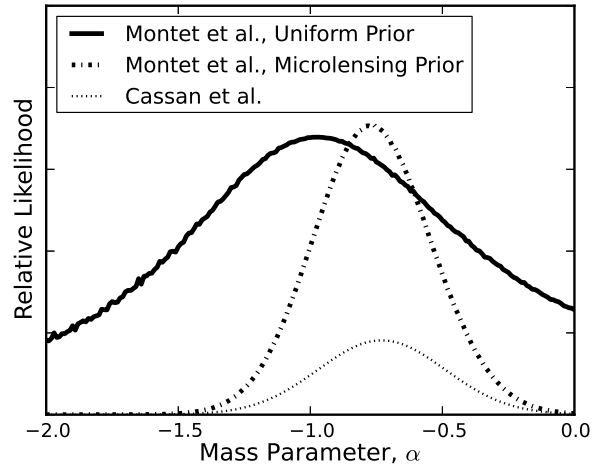


FIG. 13.— Relative likelihood values for the mass parameter α , assuming the planets in our sample and microlensing systems are members of the same population. We find a maximum likelihood value of $\alpha = -0.94 \pm 0.56$, consistent with values of α found from analyses of microlensing planets but steeper than previous RV results for FGK stars at 1.1σ . This result may suggest the planet distribution function is different for M stars as compared to higher mass stars. When we include the Cassan et al. (2012) result as a prior on our measurement, we find $\alpha = -0.77 \pm 0.22$.

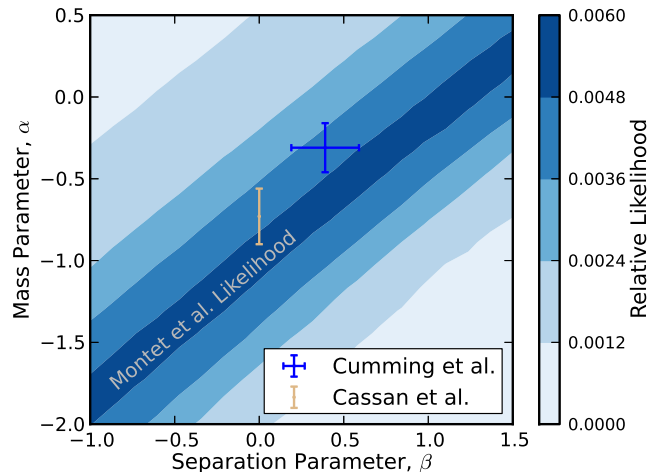


FIG. 14.— Relative likelihood values for the mass parameter α , and separation parameter β . There is a maximum likelihood contour approximately along the line $\alpha - \beta = -1$, suggesting a relationship between the two parameters required to fit both our result and the microlensing results, assuming the local planets in our sample and microlensing systems are members of the same population. Points included in the plot are the Cumming et al. (2008) RV result (blue) and the Cassan et al. (2012) microlensing result (cyan), the latter of which assumes an Öpik’s Law value of $\beta = 0$. The small discrepancy between our result and the Cumming et al. (2008) result may suggest the planet distribution function may differ between M-dwarfs and FGK stars.

in the range $-1.0 < \beta < 1.0$, consistent with the assumptions from previous microlensing studies, and allow our mass parameter to be any value subject to the constraints of Fig. 14. By weighting our occurrence rates found in §4.6 in this manner, we find a most likely occurrence rate of $7.2 \pm 3.1\%$, consistent with that found by assuming the power-law distribution of Cumming et al. (2008). As the measured planet frequency depends on the distribution

function parameters, an improved value of the planet occurrence rate, either by this method, microlensing, or through astrometry measured by *Gaia* (Casertano et al. 2008), will provide immediate constraints on the distribution function of giant planets. Similarly, improved constraints on the distribution parameters will enable an immediate improvement of the determination of the giant planet occurrence rate.

The Cumming et al. (2008) power-law parameters α and β are less consistent with our results. This may suggest the planet distribution function around FGK stars is systematically different from the planet distribution function around M-dwarfs. As Bowler et al. (2010) find an even larger value for α in their study of retired A stars (excluding all $\alpha < 0$), which matches comparison studies between RV surveys and high-contrast imaging searches (Crepp & Johnson 2011), this possibility is certainly plausible. With additional M-dwarfs targeted by a combination of RV observations with longer time baselines and high-contrast imaging to improve the estimate of the occurrence rate, we will be able to directly probe this possibility.

5. SUMMARY AND CONCLUSION

We have analyzed a collection of 111 nearby M-dwarfs observed in RV surveys with a median time baseline of 11.8 years in a search for long-term RV accelerations. We have developed a new technique to determine the incidence of giant planets in which we target systems with such accelerations using adaptive optics imaging to “peer beyond the horizon” set by Doppler time baselines. With a relatively short exposure image using the Keck AO system, we can eliminate the possibility of binary stellar companions and massive brown dwarfs. We conclude with high statistical confidence that accelerations without a directly imaged companion are likely caused by a planet in a wide orbit.

Accounting for false positive and false negative rates, we find that $6.5 \pm 3.0\%$ of M-dwarfs host a giant planet with mass $1 < m/M_J < 13$ and semimajor axis $a < 20$ AU, assuming such planets are distributed following the power-law parameters estimated by Cumming et al. (2008). The exact integrated planet occurrence rate does not depend strongly on the distribution function parameters chosen. We find evidence for a correlation between giant planet frequency and stellar metallicity, similar to that observed in the RV-detected planet population. Additional follow-up work confirming this result would suggest giant planets in wide orbits may form in the same way as the RV-detected giant planets. Observations of more stars are needed to determine if a correlation exists between planet occurrence at wide separations and stellar mass inside of the M-dwarf spectral class.

Our overall occurrence rate is consistent with what might be expected based on the results of microlensing planet search surveys, but microlensing overpredicts the number of giant planets near the Einstein radius if the underlying planet distribution found by Cumming et al. (2008) for FGK stars is assumed. Namely, if the giant planet distribution is given as a double power law, such that $d^2N \propto M^\alpha a^\beta d \ln M d \ln a$, with $\alpha = -0.31 \pm 0.20$ and $\beta = 0.39 \pm 0.15$, then microlensing studies overestimate the giant planet occurrence rate. From our bulk occurrence rate, we determine an expected planet de-

tection rate for microlensing studies which depends on our chosen planet distribution function. By assuming an Öpik’s Law distribution (i.e., flat in $\log a$), the microlensing planet occurrence rate is consistent with our result if the planet population is represented by the power-law $dN \propto m^{-0.94 \pm 0.56} d \log m$. This value for α is consistent with previous M-dwarf studies conducted by microlensing planet search teams (Gould et al. 2010; Cassan et al. 2012). We also find other non-Öpik distributions can be chosen to simultaneously explain our results and the microlensing results; these fall approximately on the line $\alpha - \beta = -1$, where α and β are planet distribution power-law indices defined in Eq. 6. Moreover, an improved estimate of the giant planet occurrence rate, as measured by *Gaia*, can be combined with our results to provide enhanced constraints on α and β .

Our knowledge of planets around M-dwarfs has significantly improved in the last few years thanks to both targeted RV searches and high contrast imaging campaigns (Apps et al. 2010; Bowler et al. 2012). As such surveys continue, they will begin to confirm and characterize planets in wider orbits, pushing into the domain currently only studied by microlensing studies. To directly compare these populations, understanding the properties of host stars to planets found by microlensing will be extremely important; when possible, every effort should be made to collect spectroscopic followup data on microlensing events to determine the physical properties of lens host stars to better understand both the planet population around M-dwarfs and how it changes across the galaxy.

The method developed in this paper can be extended to higher-mass stars with little difficulty. For example, a large sample of K-dwarfs has been observed by the CPS collaboration. This sample is larger, has more observations, and exhibits less astrophysical jitter than our M-dwarf sample; all of these factors improve our ability to detect RV accelerations. However, the stars are more luminous and on average more distant, complicating adaptive optics searches. Care must be taken to ensure low-mass stellar companions are accounted for, as adaptive optics imaging may not be sensitive to all M-dwarf companions to K-dwarfs without longer observations or the use of ADI. In the future, we intend to apply this technique to the CPS K-dwarfs to determine the planet occurrence rate around higher mass stars and compare to the M-dwarfs.

Most of the data presented herein were obtained at the W.M. Keck Observatory, which is operated as a scientific partnership among the California Institute of Technology, the University of California and the National Aeronautics and Space Administration. The Observatory was made possible by the generous financial support of the W.M. Keck Foundation. We made use of the SIMBAD database operated at CDS, Strasbourg, France, and NASA’s Astrophysics Data System Bibliographic Services. We thank Jon Swift for collecting NIRC2 observations of HIP 57050. We also thank Brendan Bowler for helpful comments on an early version of this manuscript. B.T.M. is supported by the National Science Foundation Graduate Research Fellowship under Grant No. DGE1144469. The TRENDS high-contrast

imaging program is supported by NASA Origins grant NNX13AB03G. J.A.J. is supported by generous grants from the David and Lucile Packard Foundation and the Alfred P. Sloan Foundation. B.T.M. would also like to thank the Statistical and Applied Mathematical Sciences Institute; conversations at the June 2013 Modern Statistical and Computational Methods for Analysis of Kepler Data workshop at SAMSI improved the final version of

this manuscript.

Finally, the authors wish to recognize and acknowledge the very significant cultural role and reverence that the summit of Mauna Kea has always had within the indigenous Hawaiian community. We are most fortunate to have the opportunity to conduct observations from this mountain.

REFERENCES

- Abell, G. O. 1959, *Leaflet of the Astronomical Society of the Pacific*, 8, 121, 121
- Anglada-Escudé, G., Boss, A. P., Weinberger, A. J., et al. 2012a, *ApJ*, 746, 37, 37
- Anglada-Escudé, G., Arriagada, P., Vogt, S. S., et al. 2012b, *ApJ*, 751, L16, L16
- Apps, K., Clubb, K. I., Fischer, D. A., et al. 2010, *PASP*, 122, 156, 156
- Baraffe, I., Chabrier, G., Barman, T. S., Allard, F., & Hauschildt, P. H. 2003, *A&A*, 402, 701, 701
- Batalha, N. M., Rowe, J. F., Bryson, S. T., et al. 2013, *ApJS*, 204, 24, 24
- Bean, J. L., Sneden, C., Hauschildt, P. H., Johns-Krull, C. M., & Benedict, G. F. 2006, *ApJ*, 652, 1604, 1604
- Beuzit, J.-L., Ségransan, D., Forveille, T., et al. 2004, *A&A*, 425, 997, 997
- Bonfils, X., Delfosse, X., Udry, S., et al. 2013, *A&A*, 549, A109, A109
- Borucki, W. J., & Summers, A. L. 1984, *Icarus*, 58, 121, 121
- Borucki, W. J., Koch, D., Basri, G., et al. 2010, *Science*, 327, 977, 977
- Bowler, B. P., Liu, M. C., Shkolnik, E. L., et al. 2012, *ApJ*, 753, 142, 142
- Bowler, B. P., Johnson, J. A., Marcy, G. W., et al. 2010, *ApJ*, 709, 396, 396
- Browning, M. K., Basri, G., Marcy, G. W., West, A. A., & Zhang, J. 2010, *AJ*, 139, 504, 504
- Butler, R. P., Johnson, J. A., Marcy, G. W., et al. 2006, *PASP*, 118, 1685, 1685
- Campo, C. J., Harrington, J., Hardy, R. A., et al. 2011, *ApJ*, 727, 125, 125
- Carson, J., Thalmann, C., Janson, M., et al. 2013, *ApJ*, 763, L32, L32
- Casertano, S., Lattanzi, M. G., Sozzetti, A., et al. 2008, *A&A*, 482, 699, 699
- Cassan, A., Kubas, D., Beaulieu, J.-P., et al. 2012, *Nature*, 481, 167, 167
- Chabrier, G., Baraffe, I., Allard, F., & Hauschildt, P. 2000, *ApJ*, 542, 464, 464
- Chang, C.-K., Ko, C.-M., & Peng, T.-H. 2011, *ApJ*, 740, 34, 34
- Choi, J., McCarthy, C., Marcy, G. W., et al. 2013, *ApJ*, 764, 131, 131
- Crepp, J. R., & Johnson, J. A. 2011, *ApJ*, 733, 126, 126
- Crepp, J. R., Johnson, J. A., Howard, A. W., et al. 2013, *ArXiv e-prints*, arXiv:1305.0571
- Crepp, J. R., Johnson, J. A., Fischer, D. A., et al. 2012a, *ApJ*, 751, 97, 97
- Crepp, J. R., Johnson, J. A., Howard, A. W., et al. 2012b, *ApJ*, 761, 39, 39
- Cumming, A., Butler, R. P., Marcy, G. W., et al. 2008, *PASP*, 120, 531, 531
- Cutri, R. M., Skrutskie, M. F., van Dyk, S., et al. 2003, *Delfosse, X., Forveille, T., Ségransan, D., et al. 2000, A&A*, 364, 217, 217
- Dieterich, S. B., Henry, T. J., Golimowski, D. A., Krist, J. E., & Tanner, A. M. 2012, *AJ*, 144, 64, 64
- Dressing, C. D., & Charbonneau, D. 2013, *ApJ*, 767, 95, 95
- Dupuy, T. J., Liu, M. C., Bowler, B. P., et al. 2010, *ApJ*, 721, 1725, 1725
- Faherty, J. K., Burgasser, A. J., Cruz, K. L., et al. 2009, *AJ*, 137, 1, 1
- Femenía, B., Rebolo, R., Pérez-Prieto, J. A., et al. 2011, *MNRAS*, 413, 1524, 1524
- Fischer, D. A., & Marcy, G. W. 1992, *ApJ*, 396, 178, 178
- Fischer, D. A., & Valenti, J. 2005, *ApJ*, 622, 1102, 1102
- Fischer, D. A., Gaidos, E., Howard, A. W., et al. 2012, *ApJ*, 745, 21, 21
- Foreman-Mackey, D., Hogg, D. W., Lang, D., & Goodman, J. 2013, *PASP*, 125, 306, 306
- Gatewood, G. 2008, *AJ*, 136, 452, 452
- Gaudi, B. S., Seager, S., & Mallen-Ornelas, G. 2005, *ApJ*, 623, 472, 472
- Gaudi, B. S., Albrow, M. D., An, J., et al. 2002, *ApJ*, 566, 463, 463
- Gaudi, B. S., Bennett, D. P., Udalski, A., et al. 2008, *Science*, 319, 927, 927
- Gliese, W., & Jahreiß, H. 1991, *Preliminary Version of the Third Catalogue of Nearby Stars*
- Goldman, B., Marsat, S., Henning, T., Clemens, C., & Greiner, J. 2010, *MNRAS*, 405, 1140, 1140
- Golimowski, D. A., Henry, T. J., Krist, J. E., et al. 2004, *AJ*, 128, 1733, 1733
- Gomes da Silva, J., Santos, N. C., Bonfils, X., et al. 2012, *A&A*, 541, A9, A9
- Gould, A., Dong, S., Gaudi, B. S., et al. 2010, *ApJ*, 720, 1073, 1073
- Gray, D. F. 1988, *Henry, T. J., Jao, W.-C., Subasavage, J. P., et al. 2006, AJ*, 132, 2360, 2360
- Ho, S., & Turner, E. L. 2011, *ApJ*, 739, 26, 26
- Holman, M. J., & Wiegert, P. A. 1999, *AJ*, 117, 621, 621
- Howard, A. W., Johnson, J. A., Marcy, G. W., et al. 2010a, *ApJ*, 721, 1467, 1467
- Howard, A. W., Marcy, G. W., Johnson, J. A., et al. 2010b, *Science*, 330, 653, 653
- Howard, A. W., Marcy, G. W., Bryson, S. T., et al. 2012, *ApJS*, 201, 15, 15
- Isaacson, H., & Fischer, D. 2010, *ApJ*, 725, 875, 875
- Jeffreys, H. 1961, *Theory of Probability*
- Jenkins, J. S., Ramsey, L. W., Jones, H. R. A., et al. 2009, *ApJ*, 704, 975, 975
- Johnson, J. A. 2009, *PASP*, 121, 309, 309
- Johnson, J. A., Aller, K. M., Howard, A. W., & Crepp, J. R. 2010a, *PASP*, 122, 905, 905
- Johnson, J. A., & Apps, K. 2009, *ApJ*, 699, 933, 933
- Johnson, J. A., Howard, A. W., Marcy, G. W., et al. 2010b, *PASP*, 122, 149, 149
- Johnson, J. A., Gazak, J. Z., Apps, K., et al. 2012, *AJ*, 143, 111, 111
- Kaib, N. A., Raymond, S. N., & Duncan, M. 2013, *Nature*, 493, 381, 381
- Kalas, P., Graham, J. R., Chiang, E., et al. 2008, *Science*, 322, 1345, 1345
- Khrutskaya, E. V., Izmailov, I. S., & Khovrichiev, M. Y. 2010, *Astronomy Letters*, 36, 576, 576
- Koch, D. G., Borucki, W. J., Basri, G., et al. 2010, *ApJ*, 713, L79, L79
- Kraus, A. L., & Ireland, M. J. 2012, *ApJ*, 745, 5, 5
- Kuzuhara, M., Tamura, M., Kudo, T., et al. 2013, *ArXiv e-prints*, arXiv:1307.2886
- Lagrange, A.-M., Gratadour, D., Chauvin, G., et al. 2009, *A&A*, 493, L21, L21
- Liu, M. C., Fischer, D. A., Graham, J. R., et al. 2002, *ApJ*, 571, 519, 519
- Lloyd, J. P. 2002, *PhD thesis*
- Luhman, K. L. 2012, *ARA&A*, 50, 65, 65
- Mann, A. W., Gaidos, E., Lépine, S., & Hilton, E. J. 2012, *ApJ*, 753, 90, 90

- Marcy, G. W., & Butler, R. P. 2000, *PASP*, 112, 137, 137
- Marois, C., Macintosh, B., Barman, T., et al. 2008, *Science*, 322, 1348, 1348
- Marois, C., Zuckerman, B., Konopacky, Q. M., Macintosh, B., & Barman, T. 2010, *Nature*, 468, 1080, 1080
- Metchev, S. A., & Hillenbrand, L. A. 2009, *ApJS*, 181, 62, 62
- Morton, T. D., & Swift, J. J. 2013, *ArXiv e-prints*, arXiv:1303.3013
- Nakajima, T., Oppenheimer, B. R., Kulkarni, S. R., et al. 1995, *Nature*, 378, 463, 463
- Napiwotzki, R. 2009, *Journal of Physics Conference Series*, 172, 012004, 012004
- Neves, V., Bonfils, X., Santos, N. C., et al. 2012, *A&A*, 538, A25, A25
- Nielsen, E. L., & Close, L. M. 2010, *ApJ*, 717, 878, 878
- Ópik, E. 1924, *Pulications de L'Observatoire Astronomique de l'Université de Tartu*, 25, 6, 6
- Peña Ramírez, K., Béjar, V. J. S., Zapatero Osorio, M. R., Petr-Gotzens, M. G., & Martín, E. L. 2012, *ApJ*, 754, 30, 30
- Pedicelli, S., Bono, G., Lemasle, B., et al. 2009, *A&A*, 504, 81, 81
- Rameau, J., Chauvin, G., Lagrange, A.-M., et al. 2013, *ApJ*, 772, L15, L15
- Rauscher, E., & Marcy, G. W. 2006, *PASP*, 118, 617, 617
- Reid, I. N., & Cruz, K. L. 2002, *AJ*, 123, 2806, 2806
- Robinson, S. E., Laughlin, G., Vogt, S. S., et al. 2007, *ApJ*, 670, 1391, 1391
- Rojas-Ayala, B., Covey, K. R., Muirhead, P. S., & Lloyd, J. P. 2010, *ApJ*, 720, L113, L113
- Rolleston, W. R. J., Smartt, S. J., Dufton, P. L., & Ryans, R. S. I. 2000, *A&A*, 363, 537, 537
- Scholz, R.-D. 2010, *A&A*, 515, A92, A92
- Schwarz, G. 1978, *The Annals of Statistics*, 6, 461, 461
- Siegler, N., Close, L. M., Mamajek, E. E., & Freed, M. 2003, *ApJ*, 598, 1265, 1265
- Skrutskie, M. F., Cutri, R. M., Stiening, R., et al. 2006, *AJ*, 131, 1163, 1163
- Stevenson, K. B., Harrington, J., Fortney, J. J., et al. 2012, *ApJ*, 754, 136, 136
- Sumi, T., Bennett, D. P., Bond, I. A., et al. 2010, *ApJ*, 710, 1641, 1641
- Sumi, T., Kamiya, K., Bennett, D. P., et al. 2011, *Nature*, 473, 349, 349
- Swift, J. J., Johnson, J. A., Morton, T. D., et al. 2013, *ApJ*, 764, 105, 105
- van Altena, W. F., Lee, J. T., & Hoffleit, E. D. 1995, *van Leeuwen, F.* 2007, *A&A*, 474, 653, 653
- Vigan, A., Patience, J., Marois, C., et al. 2012, *A&A*, 544, A9, A9
- Vogt, S. S., Allen, S. L., Bigelow, B. C., et al. 1994, in *Society of Photo-Optical Instrumentation Engineers (SPIE) Conference Series*, Vol. 2198, Society of Photo-Optical Instrumentation Engineers (SPIE) Conference Series, ed. D. L. Crawford & E. R. Craine, 362
- Wheeler, J. C. 2012, *ApJ*, 758, 123, 123
- Winn, J. N. 2011, *Exoplanet Transits and Occultations*, ed. S. Piper, 55–77
- Wizinowich, P., Acton, D. S., Shelton, C., et al. 2000, *PASP*, 112, 315, 315
- Wright, J. T. 2005, *PASP*, 117, 657, 657
- Wright, J. T., Marcy, G. W., Howard, A. W., et al. 2012, *ApJ*, 753, 160, 160
- Wright, J. T., Marcy, G. W., Fischer, D. A., et al. 2007, *ApJ*, 657, 533, 533
- Wright, J. T., Veras, D., Ford, E. B., et al. 2011, *ApJ*, 730, 93, 93
- Youdin, A. N. 2011, *ApJ*, 742, 38, 38

TABLE 1
M-DWARF STARS ANALYZED IN THIS STUDY

Star	RA	Dec	Mass (M_{\odot})	[Fe/H]	Spectral Type	V	d (pc)	N_{obs}	Baseline (yr)	Median σ (m s^{-1})
Hip 428	00:05:10.9	+45:47:11.6	0.53	-0.07	M1	9.97	11.25	41	12.2	4.5
HD 225213	00:05:24.4	-37:21:26.5	0.39	-0.42	M1.5	8.57	4.34	67	9.9	3.4
Hip 1734	00:21:56.0	-31:24:21.8	0.55	0.09	M1.5	11.1	17.98	8	8.1	5.4
Gl 26	00:38:59.0	+30:36:58.5	0.43	0.02	M2.5	11.0	12.6 ⁵	40	11.6	4.0
Hip 3143	00:39:58.8	-44:15:11.6	0.55	-0.09	M0.5	11.4	23.99	8	9.8	6.2
Gl 48	01:02:32.2	+71:40:47.3	0.48	0.06	M3	9.96	8.24	41	15.2	2.8
Gl 49	01:02:38.9	+62:20:42.2	0.58	0.06	M1.5	9.56	9.96	22	14.2	8.0
Hip 5643	01:12:30.6	-16:59:56.3	0.13	-0.43	M4.5	12.1	3.69	15	7.1	13.6
Hip 8051	01:43:20.2	+04:19:18.0	0.41	-0.16	M2	10.9	11.41	33	12.7	3.3
Gl 83.1	02:00:13.0	+13:03:07.0	0.15	-0.31	M4.5	12.2	4.50	21	8.2	12.9
G244-047	02:01:35.3	+63:46:12.1	0.48	0.07	M3	11.0	12.76 ⁵	10	7.5	4.6
Gl 87 ¹	02:01:35.3	+63:46:12.1	0.45	-0.32	M1.5	10.0	10.41	62	13.0	2.9
Hip 11048	02:22:14.6	+47:52:48.1	0.62	-0.08	M0.5	9.34	11.94	44	12.6	5.0
Gl 105B ⁴	02:36:15.3	+06:52:19.1	0.27	-0.10	M4	11.6	7.73 ⁶	12	9.1	4.6
Gl 109	02:44:15.6	+25:31:24.1	0.35	-0.18	M3	10.5	7.51	32	13.1	3.1
Hip 21556	04:37:42.9	-11:02:19.9	0.48	-0.11	M1.5	10.3	11.10	31	12.7	2.8
Hip 22627 ¹	04:52:05.7	+06:28:35.6	0.36	0.13	M3.5	11.9	12.29	42	12.2	5.1
Hip 22762	04:59:50.0	-17:46:24.3	0.42	-0.20	M2	10.9	12.12	39	12.6	3.1
Hip 23512	05:03:20.1	-17:22:24.7	0.27	-0.25	M3	11.7	9.21	11	6.7	6.5
HD 33793	05:11:40.6	-45:01:06.3	0.27	-0.81	M1	8.89	3.91	36	13.8	3.2
Hip 24284	05:12:42.2	+19:39:56.4	0.45	-0.16	M2	10.8	12.29	30	9.1	2.7
HD 36395	05:31:27.4	-03:40:38.0	0.60	-0.05	M1.5	7.92	5.66	33	15.8	6.0
G097-054	05:34:52.1	+13:52:47.2	0.37	0.05	M3.5	11.8	12.39 ⁷	11	6.6	5.0
HD 233153	05:41:30.7	+53:29:23.3	0.60	0.05	M0.5	9.87	12.44	11	6.7	6.2
Hip 26857	05:42:09.3	+12:29:21.6	0.22	-0.24	M4	11.4	5.83	10	6.7	6.6
G192-13	06:01:11.1	+59:35:50.8	0.27	-0.11	M3.5	11.7	7.93 ⁸	16	7.8	5.9
Hip 29052	06:07:43.7	-25:44:41.5	0.30	-0.22	M4	11.8	11.35	16	7.7	5.8
Gl 226	06:10:19.8	+82:06:24.3	0.41	-0.14	M2	10.4	9.37	35	14.7	2.8
HD 42581 ³	06:10:34.6	-21:51:52.7	0.58	-0.07	M1	8.14	5.75	33	15.9	4.6
Gl 250B ⁴	06:52:18.1	-05:11:24.2	0.45	-0.12	M2	10.0	8.71	29	8.0	3.8
HD 265866	06:54:49.0	+33:16:05.4	0.35	-0.03	M3	9.89	5.59	61	14.8	2.9
Gl 273	07:27:24.5	+05:13:32.8	0.29	-0.07	M3.5	9.89	3.80	41	14.8	3.1
Hip 36338	07:28:45.4	-03:17:53.4	0.40	0.03	M3	11.4	12.29	10	10.7	3.8
Hip 36834	07:34:27.4	+62:56:29.4	0.40	-0.50	M0.5	10.8	11.47	22	6.4	6.4
Hip 37217	07:38:41.0	-21:13:28.5	0.29	-0.27	M3	11.7	10.60	11	11.8	25.9
Hip 37766	07:44:40.2	+03:33:08.8	0.31	0.27	M4.5	11.1	5.96	22	11.1	88.0
GJ 2066	08:16:08.0	+01:18:09.3	0.46	-0.10	M2	10.0	9.12	37	14.8	2.9
Gl 317 ^{1,2}	08:40:59.2	-23:27:23.3	0.43	0.20	M3.5	13.0	15.31 ⁹	45	12.1	5.0
HD 75732B ⁴	08:52:40.8	+28:18:59.0	0.27	0.15	M4	13.1	13.02 ¹⁰	21	9.1	7.2
Hip 46655	09:30:44.6	+00:19:21.6	0.29	-0.17	M3.5	11.7	9.67	11	6.0	4.8
Hip 46769	09:31:56.3	+36:19:12.8	0.53	-0.27	M0	10.1	13.91	23	8.0	3.7
Gl 357	09:36:01.6	-21:39:38.9	0.33	-0.31	M2.5	10.9	9.02	36	14.2	2.8
Hip 47513	09:41:10.4	+13:12:34.4	0.48	-0.12	M1.5	10.4	11.26	29	12.1	4.1
Hip 47650	09:42:51.7	+70:02:21.9	0.41	0.13	M3	11.2	11.35	10	6.2	16.5
Hip 48714	09:56:08.7	+62:47:18.5	0.64	-0.03	M0	9.00	10.56	16	11.2	6.5
Gl 382	10:12:17.7	-03:44:44.4	0.54	0.02	M1.5	9.26	7.87	29	12.9	5.5
Gl 388	10:19:36.3	+19:52:10.1	0.41	0.10	M3.5	9.43	4.69 ⁶	39	5.7	24.1
Hip 51007	10:25:10.8	-10:13:43.3	0.54	-0.07	M1	10.1	12.35	19	11.1	4.8
Gl 393	10:28:55.6	+00:50:27.6	0.44	-0.14	M2	9.63	7.07	42	14.4	3.5
Hip 53020	10:50:52.0	+06:48:29.2	0.26	0.00	M4	11.6	6.76	12	6.3	7.3
Gl 406	10:56:28.9	+07:00:52.8	0.10	0.22	M5.5	13.5	2.39	21	13.0	20.5
Gl 408	11:00:04.3	+22:49:58.6	0.38	-0.15	M2.5	10.0	6.66	39	14.8	3.4
HD 95650	11:02:38.3	+21:58:01.7	0.59	-0.10	M0	9.57	11.77	30	11.1	10.9
HD 95735	11:03:20.2	+35:58:11.6	0.39	-0.32	M2	7.49	2.55	211	15.2	2.8
Hip 54532	11:09:31.3	-24:35:55.1	0.46	-0.08	M2	10.4	10.75	26	12.2	3.9
HD 97101B ⁴	11:11:01.9	+30:26:44.4	0.58	0.52	M1.5	9.95	11.87	25	10.5	4.9
Hip 55360	11:20:04.8	+65:50:47.3	0.49	-0.35	M0	9.32	8.92	30	11.9	3.3
Gl 433	11:35:26.9	-32:32:23.9	0.47	-0.15	M1.5	9.79	8.88	27	13.1	3.4
Hip 57050 ^{1,2}	11:41:44.6	+42:45:07.1	0.35	0.08	M4	12.0	11.10	40	11.8	4.6
Hip 57087 ²	11:42:11.2	+26:42:22.6	0.44	-0.03	M2.5	10.6	10.14	257	12.0	2.8
Gl 445	11:47:41.4	+78:41:28.2	0.25	-0.27	M3.5	10.7	5.35	48	13.3	2.9
Hip 57548	11:47:44.4	+00:48:16.4	0.17	-0.23	M4	11.0	3.36	17	12.8	9.6
Gl 450	11:51:07.3	+35:16:19.3	0.46	-0.21	M1	9.78	8.59	31	14.1	5.1
Hip 59406 ⁴	12:11:11.8	-19:57:38.1	0.35	-0.13	M3	11.6	12.59	11	7.0	4.9
Hip 59406b ⁴	12:11:17.0	-19:58:21.4	0.25	-0.25	M4	12.1	12.59	12	6.2	6.9
Hip 60559	12:24:52.5	-18:14:32.2	0.26	-0.56	M4	11.3	8.85	14	6.3	4.6
Gl 486	12:47:56.6	+09:45:05.0	0.32	0.01	M3.5	11.4	8.37	20	8.2	3.8
Gl 514	13:29:59.8	+10:22:37.8	0.53	-0.15	M0.5	9.04	7.66	50	13.9	3.8
HD 119850	13:45:43.8	+14:53:29.5	0.50	-0.16	M1.5	8.46	5.39	42	13.9	2.5
Hip 67164	13:45:50.7	-17:58:05.6	0.31	-0.06	M3.5	11.8	10.24	14	6.2	4.6
HD 122303	14:01:03.2	-02:39:17.5	0.52	-0.16	M1	9.72	10.03	37	11.8	3.6
Hip 70865 ¹	14:29:29.7	+15:31:57.5	0.52	0.00	M2	10.6	14.00	21	8.5	3.3
Hip 70975	14:31:01.2	-12:17:45.9	0.32	-0.05	M3.5	11.9	10.82	15	11.3	4.1
Hip 71253	14:34:16.8	-12:31:10.4	0.28	0.11	M4	11.3	6.06	21	7.9	4.9

TABLE 1 — Continued

Star	RA	Dec	Mass (M_{\odot})	[Fe/H]	Spectral Type	V	d (pc)	N_{obs}	Baseline (yr)	Median σ (m s^{-1})
Gl 569A	14:54:29.2	+16:06:03.8	0.48	-0.03	M2.5	10.2	9.65	13	5.1	15.0
Hip 74995 ²	15:19:27.5	-07:43:19.4	0.30	-0.18	M3	10.5	6.21	197	12.5	3.1
HD 147379B ⁴	16:16:45.3	+67:15:22.5	0.47	0.09	M3	10.6	10.74	14	5.9	4.6
Gl 625	16:25:24.6	+54:18:14.7	0.32	-0.39	M1.5	10.1	6.52	48	14.0	3.2
Hip 83043 ²	16:58:08.9	+25:44:39.0	0.54	-0.10	M1	9.62	10.34	50	12.6	5.8
Hip 83762	17:07:07.5	+21:33:14.5	0.38	-0.10	M3	11.6	13.4	8	2.9	3.0
Hip 84099	17:11:34.7	+38:26:33.9	0.38	-0.05	M3.5	11.5	12.00	16	6.2	3.8
Hip 84790	17:19:52.7	+41:42:49.7	0.37	-0.21	M2.5	11.3	12.38	17	4.9	3.7
Gl 687	17:36:25.9	+68:20:20.9	0.40	-0.06	M3	9.15	4.53	100	13.8	2.6
Gl 686	17:37:53.3	+18:35:30.2	0.44	-0.31	M1	9.62	8.09	60	14.4	2.7
Gl 694	17:43:56.0	+43:22:43.0	0.44	-0.02	M2.5	10.5	9.48	38	14.4	3.8
Gl 699	17:57:48.5	+04:41:36.2	0.16	-0.61	M4	9.54	1.82	230	15.3	7.1
HD 165222	18:05:07.6	-03:01:52.8	0.48	-0.22	M1	9.37	7.76	142	14.4	3.3
G205-028	18:31:58.4	+40:41:10.4	0.31	-0.14	M3.5	11.9	11.9 ¹¹	12	6.2	27.8
GJ 4063	18:34:36.6	+40:07:26.4	0.19	-0.61	M3.5	11.4	7.25 ¹⁰	14	6.9	3.7
Hip 91699 ¹	18:41:59.0	+31:49:49.8	0.37	-0.13	M3	11.2	11.45	17	12.0	4.5
Hip 92403	18:49:49.4	-23:50:10.4	0.17	-0.43	M3.5	10.9	2.97	27	8.1	8.2
Gl 745A ⁴	19:07:05.6	+20:53:17.0	0.30	-0.48	M1.5	10.7	8.51	26	13.3	3.3
Gl 745B ⁴	19:07:13.2	+20:52:37.2	0.31	-0.45	M1.5	10.7	8.75	21	10.4	3.8
G207-019	19:08:30.0	+32:16:52.0	0.34	-0.10	M3	11.8	12.39 ¹¹	12	6.2	10.3
HD 180617 ⁴	19:16:55.3	+05:10:08.1	0.48	0.02	M2.5	9.13	5.87	143	9.8	3.5
Gl 793	20:30:32.0	+65:26:58.4	0.38	-0.03	M2.5	10.4	8.00	30	14.2	5.2
Gl 806	20:45:04.1	+44:29:56.7	0.44	-0.16	M1.5	10.7	12.32	63	15.3	3.4
Hip 103039	20:52:33.0	-16:58:29.0	0.23	-0.10	M4	11.4	5.71	19	8.2	6.5
HD 199305	20:53:19.8	+62:09:15.8	0.58	-0.02	M0.5	8.54	7.05	45	15.3	4.6
Hip 104432	21:09:17.4	-13:18:09.0	0.36	-0.51	M1	10.8	12.17	34	12.3	3.5
HD 209290	22:02:10.3	+01:24:00.8	0.60	-0.10	M0	9.16	10.24	56	11.0	4.7
Hip 109388 ^{1,2}	22:09:40.3	-04:38:26.6	0.49	0.22	M3.5	10.4	9.10	84	14.4	3.5
Hip 109555	22:11:30.1	+18:25:34.3	0.55	0.13	M2	10.4	11.62	16	11.1	6.2
Gl 876 ²	22:53:16.7	-14:15:49.3	0.34	0.13	M4	10.1	4.69	207	14.4	4.5
HD 216899 ⁴	22:56:34.8	+16:33:12.4	0.58	0.03	M1.5	8.66	6.84	50	15.1	4.3
HD 217987	23:05:52.0	-35:51:11.0	0.47	-0.33	M0.5	7.34	3.28	69	14.3	3.5
Hip 114411	23:10:15.7	-25:55:52.7	0.46	-0.13	M2	11.2	16.08	11	8.9	4.3
Hip 115332	23:21:37.4	+17:17:25.4	0.40	0.27	M4	11.7	10.99	14	6.7	4.6
Hip 115562	23:24:30.5	+57:51:15.5	0.59	0.08	M1	10.0	12.96	10	8.8	6.4
Gl 905	23:41:55.0	+44:10:40.8	0.14	0.05	M5	12.2	3.16 ¹²	17	8.0	32.8
Gl 908	23:49:12.5	+02:24:04.4	0.42	-0.39	M1	8.98	5.98	89	16.0	2.9

NOTE. — All distance measurements, unless otherwise listed, are taken from the parallax measurements listed in van Leeuwen (2007). 1—RV acceleration observed

2—Confirmed planetary-mass companion

3—Confirmed brown dwarf companion

4—Wide binary companion

Metallicity uncertainties are taken to be 0.17 dex, while mass uncertainties are taken as 10%, following the method of Delfosse et al. (2000)

¹ RV acceleration observed

² Confirmed Planetary Mass Companion

³ Confirmed Brown Dwarf Companion

⁴ Wide Binary Companion

⁵ van Altena et al. (1995)

⁶ Jenkins et al. (2009)

⁷ Gliese & Jahreiß (1991)

⁸ Khrutskaya et al. (2010)

⁹ Anglada-Escudé et al. (2012a)

¹⁰ Reid & Cruz (2002)

¹¹ Browning et al. (2010)

¹² Gatewood (2008)

TABLE 2
STARS WITH MEASURED RV ACCELERATIONS

Star	RV Slope (m s ⁻¹ yr ⁻¹)	AO Observation Date	Instrument	Filter	ADI
Gl 317	2.51 ± 0.62 ²	2010 October 13	NIRC2	<i>K'</i>	Yes
Hip 22627	-1.17 ± 0.29	2012 February 2	NIRC2	<i>K'</i>	Yes
Hip 57050	1.39 ± 0.39	2012 December 27	NIRC2	<i>K_s</i>	No
Hip 109388	N/A ²	2011 June 24	NIRC2	<i>L</i>	Yes
Hip 63510 ¹	N/A ²	N/A	N/A	N/A	N/A
Hip 71898 ¹	8.6 ± 0.4	N/A	N/A	N/A	N/A

APPENDIX

NOTES ON INDIVIDUAL TARGETS

HIP 109388

The RV data for HIP 109388 exhibits a clear planetary signal from the known companion HIP 109388b. The residuals to the best-fitting orbit for this planet exhibit strong curvature, motivating our two-planet fit. Moreover, there is no correlation between this long period signal and stellar magnetic activity, suggesting the planet is not the result of an apparent velocity change during the star’s magnetic cycle. To determine the orbital parameters of both planets, we utilize emcee, an affine invariant MCMC ensemble sampler (Foreman-Mackey et al. 2013). For both planets, we fit five orbital parameters: the eccentricity e , argument of periastron ω , time at which a transit would occur $t_{\varpi=90}$, Doppler semi-amplitude K (or the product of the planet mass and the inclination $m \sin i$), and planet orbital period P . We also include the systemic radial velocity γ as a free parameter, as well as a velocity offset between observations taken before August 18, 2004 and after that date, corresponding to an upgrade of the HIRES CCD detector (Wright et al. 2011).

Due to the curvature in the outer planet’s orbit, we are able to constrain the mass and period of both companions. As shown in Fig. 15, the orbit of the outer planet is only weakly constrained. Nevertheless, the data can rule out orbits with $m \sin i > 2.5M_J$. Moreover, we refine the inner planet’s parameters: we find the “b” component’s best-fitting mass and period increase slightly, but the distributions for each are consistent with those found by Butler et al. (2006). Our parameters for each planet are included in Table 3.

TABLE 3
ORBITAL PARAMETERS FOR HIP 109388

Parameter	Mean	50%	15.8%	84.2%
<i>Planet b</i>				
Orbital period P (yr)	5.2411	5.2425	-0.0672	+0.0637
Planet mass ¹ $m \sin i$ (M_J)	.89892	0.89974	-0.0449	+0.0432
Time of potential transit $t_{\varpi=90}$ (JD-2440000)	537.34	536.86	-161.26	+164.73
$e^{1/2} \cos \omega$	-0.0483	-0.0548	-0.1049	+0.1216
$e^{1/2} \sin \omega$	0.0985	0.1160	-0.1612	+0.1135
<i>Planet c</i>				
Orbital period P (yr)	24.043	19.346	-5.931	+17.204
Planet mass ¹ $m \sin i$ (M_J)	0.7725	0.7022	-0.2034	+0.3436
Time of potential transit $t_{\varpi=90}$ (JD-2440000)	3586.3	5660.3	-7356.0	+2387.6
$e^{1/2} \cos \omega$	-0.3108	-0.3457	-0.1849	+0.2598
$e^{1/2} \sin \omega$	-0.3483	-0.3611	-0.2344	+0.2526
<i>System Parameters</i>				
HIRES detector upgrade offset (m s ⁻¹)	17.071	17.183	-5.248	+5.012

HIP 109555

When observing HIP 109555 we detected a possible faint companion object located tens of arcseconds away. To prove this companion is not associated with the primary but is instead unrelated, we compare the proper motion of both objects by identifying them in the 2MASS catalog (Skrutskie et al. 2006) and the Palomar Observatory Sky Survey (Abell 1959). Comparing the POSS data collected 16 July 1950 to the 2MASS observation, we detect a proper motion for HIP 109555 of 0.36 arcsec/yr, consistent with previously published results. The hypothetical companion motion, however, is only 5 milliarcseconds per year. Additionally, the companion is bluer in colors derived using the 2MASS J, H, and K filters than HIP 109555. These are both consistent with the companion being a distant background object, and we neglect its presence in our analysis.

¹ Known Brown Dwarf Companion
² Curvature in RV

¹ Assuming a stellar mass of 0.49 M_{\odot}

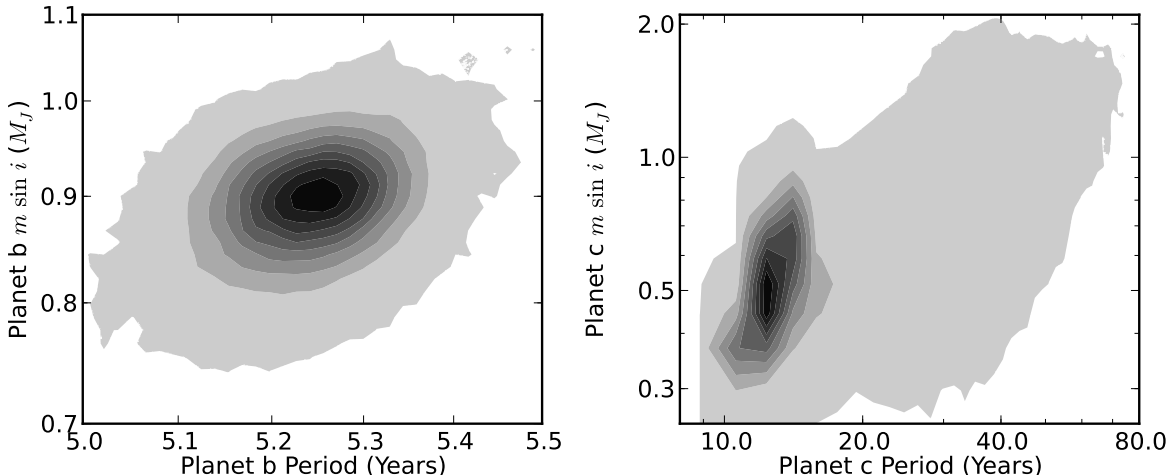


FIG. 15.— Position of (left) HIP 109388b and (right) HIP 109388c in the mass-period plane. The orbital parameters for the inner planet are much more tightly constrained than the outer planet. Both planets may have minimum masses $m \sin i > 1M_J$; depending on the exact shape of the planet distribution function; the inner planet may have more than a 50% probability of being more massive than Jupiter when orientation uncertainties are taken into account.

HIP 57050

We observed HIP 57050 (=GJ1148) on December 27, 2012 using the K_s filter on NIRC2. Our imaging is only complete at separations smaller than 1 arcsecond, corresponding to a projected separation of 11 AU. This does not enable us to rule out most stellar companions that could cause our observed RV trends, as shown in Fig. 16. If the

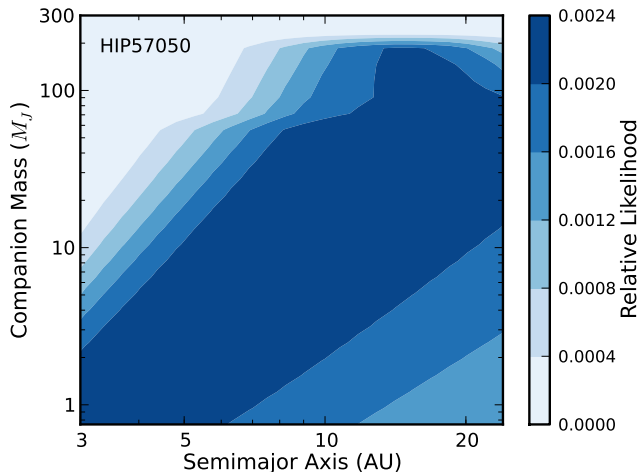


FIG. 16.— Probability contours displaying the location of a giant companion orbiting HIP 57050, given that exactly one such planet exists, when the RV data is combined with adaptive optics imaging and 2MASS data. Because the AO imagery only extends to 11 AU, there is a small region of parameter space where a low-mass M-dwarf companion could reside. Additional AO observations with a wider field of view would be required to rule out this possibility.

observed trend is caused by a stellar-mass companion, the companion is likely beyond 10 AU, which corresponds to a separation of 0.9 arcseconds. Thus any stellar companions at their maximum separation that could cause this trend would be expected to be found in a seeing-limited survey. We find no evidence for such a companion. While unlikely, additional AO observations with a wider field of view are required to fully eliminate the possibility that a low-mass star exists.

HIP 63510

HIP 63510B (Ross 458) is an M7 brown dwarf orbiting an M0.5 dwarf at approximately 3 AU (Beuzit et al. 2004). Twelve years of RV observations suggest an orbit with a period of 13.9 years, an eccentricity of 0.32, and a minimum mass $m \sin i = 67.9M_J$, suggesting a nearly edge-on orbit. We estimate a detection efficiency of 1.000 in an RV survey, which is not surprising considering the stellar RV semiamplitude is $K = 1.24 \text{ km s}^{-1}$. This system contains a second brown dwarf, which has a mass of approximately $6M_J$ and is separated from the host star by 1100 AU (Goldman et al. 2010; Scholz 2010)

HIP 71898

HIP 71898B is an L0 dwarf in a wide orbit around an M3.5 dwarf. Golimowski et al. (2004) report a projected separation of 30.01 ± 3.78 AU. This target has an RV baseline of 14 years, over which 30 observations were collected. From these observations we measure an acceleration of $8.6 \pm 0.4 \text{ m s}^{-1} \text{ yr}^{-1}$. At 30 AU, this would suggest a minimum dynamical mass $m \sin i > 45 M_J$, consistent with an L0 dwarf. A detectability plot for companions to HIP 71898 is shown in Fig. 17. The observed acceleration lies near a contour representing a 0.9 probability of RV detection, so it is not surprising this companion was detected by CPS.

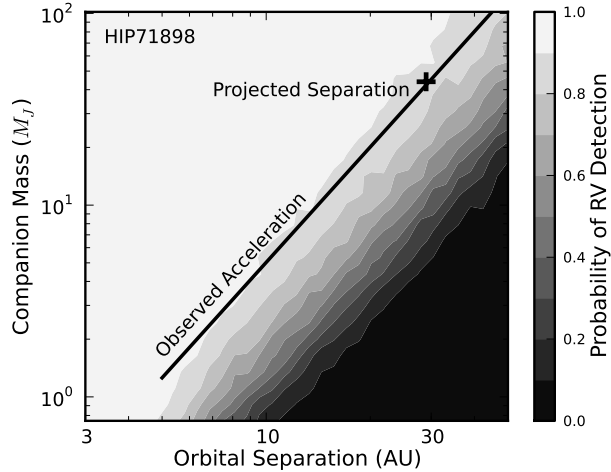


FIG. 17.— Probability contours displaying the likelihood that a planet of a given mass and semimajor axis would be detected around HIP 71898 in the CPS RV survey. The diagonal line represents companions that would produce an acceleration of $8.6 \pm 0.4 \text{ m s}^{-1} \text{ yr}^{-1}$ in an edge on system when the companion was moving along the observer’s line of sight. The X marks the spot at which a $45 M_J$ companion at 30 AU would reside; this is the minimum mass and semimajor axis expected from this companion.

G1569

G1569B is a brown dwarf binary, with an M8.5+M9 pair orbiting each other every 870 ± 9 days. The system has a combined mass of $0.140^{+0.009}_{-0.008} M_{\odot}$ (Dupuy et al. 2010) and is separated from the primary, an M3.5 dwarf, by a projected separation of 5 arcsec, or 47 AU (Femenía et al. 2011). We estimate an RV detection efficiency near zero for these companions. Thus it is not surprising that it is missed in our sample.

HD42581

HD42581B (G1229B) is a T7 dwarf at a projected separation of 44 AU (Faherty et al. 2009). This companion has been directly imaged (Nakajima et al. 1995) but not detected as a strong acceleration through RV variations. As with G1569, this object is beyond our range for efficient brown dwarf detection through RV observations, thus we should not be surprised it is not detected.